Structural Factors that Influence the Course of Overall [2 + 2] Cycloaddition Reactions between Imidozirconocene Complexes and Heterocumulenes

Rebecca L. Zuckerman and Robert G. Bergman*

Department of Chemistry, University of California, Berkeley, California 94720−1460

Received July 17, 2000

A study has been carried out to examine the factors that influence the overall [2 + 2] cycloaddition reactions between imidozirconocene complexes $Cp_2(THF)Zr{=}NR$ (R = 2,6-*i*-$Pr_2C_6H_3$, 2,6-$Me_2C_6H_3$, *t*-Bu) and small, unsaturated organic molecules. Steric factors in the cycloaddition reactions investigated were found to be significant in both the imido fragment and the heterocumulene reactant partner. When $Cp_2(THF)Zr{=}NR$ (R = 2,6-$Me_2C_6H_3$) was treated with symmetrical carbodiimides RN=C=NR (R = *t*-Bu, *i*-Pr, $SiMe_3$, cyclohexyl, *p*-tolyl), the corresponding diazametallacycles formed in high yields. However, with the more sterically encumbered zirconocene imido complex $Cp_2(THF)Zr{=}NR$ (R = 2,6-*i*-$Pr_2C_6H_3$), diazametallacycle formation was observed only with the heterocumulenes 1,3-diisopropylcarbodiimide, 1,3-dicyclohexylcarbodiimide, and 1,3-di-*p*-tolylcarbodiimide. The 16-electron diazametallacyle $Cp_2Zr(N(2,6\text{-}i\text{-}Pr_2C_6H_3)C{=}N(Tol)N(Tol))$ (**9c**) underwent rearrangement of the Zr−N bound moiety upon heating, forming a new metallacycle with the bulkier N-aryl substrate located on the exocyclic position of the four-membered zirconacycle and the less sterically demanding NR group (R = *p*-tolyl) bound to zirconium. Imido group metathesis reactions between isolated diazametallacycle complexes and carbodiimides were pursued as a method for generating new zirconium-containing metallacycles and unsymmetrical carbodiimides. When diazametallacycle $Cp_2Zr(N(t\text{-}Bu)C{=}N(SiMe_3)N(SiMe_3))$ (**7d**) was treated with an excess of bis-1,3-trimethylsilylcarbodiimide, $Cp_2Zr(N(SiMe_3)_2(N{=}C{=}NSiMe_3)$ (**13**) was obtained. The symmetrical diazametallacycle $Cp_2Zr(N(i\text{-}Pr)C{=}N(i\text{-}Pr)N(i\text{-}Pr))$ (**14**) was generated with the concurrent formation of the unsymmetrical carbodiimide *i*-PrN=C=N-*t*-Bu when diazametallacycle $Cp_2Zr(N(t\text{-}Bu)C{=}N(i\text{-}Pr)N(i\text{-}Pr))$ (**7a**) was treated with 1 equiv of 1,3-diisopropylcarbodiimide. A variable-temperature NMR experiment (−20 °C to 80 °C) revealed that complex **14** exhibits fluxional behavior with a coalescence temperature of 46 °C and a $\Delta G^{\ddagger}$ of 15.3 *k*cal/mol. This fluxionality is proposed to be due to syn/anti isomerism about the exocyclic C=N(*i*-Pr) group.

Introduction

Transition metal-mediated metathesis reactions offer many advantages over traditional approaches to the formation of new carbon−carbon/carbon−heteroatom bonds. These include milder conditions, increased reaction rates, and, in some cases, greater selectivity. Olefin metathesis catalyzed by metal carbene species has found wide utility in synthetic chemistry as a method to generate new carbon−carbon double bonds.[1−3] Extensive mechanistic work has been carried out on transition metal-mediated metathesis reactions between olefins. The accepted mechanism involves reversible [2 + 2] cycloaddition of the M=C bond across the double bond of the reactant olefin to generate a metallacyclobutane intermediate.

The exchange between multiply bonded substrates has recently been extended to the metathesis between carbon−heteroatom double bonds. In many of these reactions (stoichiometric[4−10] and catalytic[11−18]), metal-

(1) Grubbs, R. H.; Chang, S. *Tetrahedron* **1998**, *54*, 4413.
(2) Schuster, M.; Blechert, S. *Angew. Chem., Int. Ed. Engl.* **1997**, *36*, 2036.
(3) Grubbs, R. H.; Tumas, W. *Science* **1989**, *243*, 907.
(4) Meyer, K. E.; Walsh, P. J.; Bergman, R. G. *J. Am. Chem. Soc.* **1994**, *116*, 2669−2670.
(5) Meyer, K. E.; Walsh, P. J.; Bergman, R. G. *J. Am. Chem. Soc.* **1995**, *117*, 974−985.
(6) McGrane, P. L.; Livinghouse, T. *J. Am. Chem. Soc.* **1993**, *115*, 11485.
(7) Vaughan, G. A.; Hillhouse, G. L.; Lum, R. T.; Buchwald, S. L.; Rheingold, A. L. *J. Am. Chem. Soc.* **1988**, *110*, 7215.
(8) Vaughan, G. A.; Chadwick, D. S.; Hillhouse, G. L.; Rheingold, A. L. *J. Am. Chem. Soc.* **1989**, *111*, 5491.
(9) McGrane, P. L.; Jensen, M.; Livinghouse, T. *J. Am. Chem. Soc.* **1992**, *114*, 5460.
(10) Wang, W.; Espenson, J. H. *Organometallics* **1999**, *18*, 5170.
(11) Cantrell, G. K.; Meyer, T. Y. *Organometallics* **1997**, *16*, 5381.
(12) Cantrell, G. K.; Meyer, T. Y. *J. Am. Chem. Soc.* **1998**, *120*, 8035.
(13) Zuckerman, R. L.; Krska, S. W.; Bergman, R. G. *J. Am. Chem. Soc.* **2000**, *122*, 751.
(14) Krska, S. W.; Zuckerman, R. L.; Bergman, R. G. *J. Am. Chem. Soc.* **1998**, *120*, 11828.
(15) Birdwhistell, K. R.; Lanza, J.; Pasos, J. *J. Organomet. Chem.* **1999**, *584*, 200.
(16) Haak, E.; Bytschkov, I.; Doye, S. *Angew. Chem., Int. Ed. Engl.* **1999**, *38*, 3389.
(17) Baranger, A. M.; Walsh, P. J.; Bergman, R. G. *J. Am. Chem. Soc.* **1993**, *115*, 2753.
(18) Meisel, L.; Hertel, G.; Weiss, J. *J. Mol. Catal.* **1986**, *36*, 159.

10.1021/om000614c CCC: $19.00
Publication on Web 10/13/2000

lacycle complexes were initially proposed as intermediates, in analogy with the mechanisms established for olefin metathesis. However, mechanistic information for heteteroatom-containing systems at present lags behind that available for the alkene reactions. In some cases, such as the imidozirconocene system studied by Meyer, Walsh, and Bergman,[4,5] diazametallacycles have been isolated and found to undergo stoichiometric exchange reactions with imines. In addition, in the imine reactions catalyzed by these zirconocene-based systems, strong kinetic evidence has been obtained that supports a mechanism analogous to that of olefin reactions: reversible formal [2 + 2] cycloaddition reactions between the imine substrates and the active imidozirconocene catalysts, giving diazametallacyclobutane intermediates.[13,14] In other metal-mediated systems, metallacycle formation either has not been established or has been convincingly ruled out. Presumably the operating catalysts in these systems are acidic[19] or basic[20,21] species, although in most cases this has not been conclusively established. Since cycloaddition chemistry is a fundamental step in the generation of new carbon−heteroatom bonds in many systems, we decided to extend those studies to the formal [2 + 2] cycloaddition chemistry of zirconocene imido complexes with heterocumulenes.

Work done previously in our laboratory has illustrated the reactivity of the Zr=N bond in imidozirconocene complexes $Cp_2Zr{=}NR$ toward various carbonyl compounds.[22] For example, treatment of $Cp_2(THF)Zr{=}N$-*t*-Bu (**1a**) with $R_2C{=}O$ results in imido/oxo exchange to afford $R_2C{=}N$-*t*-Bu and $(Cp_2Zr{=}O)_n$ (eq 1). The imido/

$$Cp_2(THF)Zr{=}N^tBu \;(\mathbf{1a}) + R_2C{=}O \xrightarrow{-\,THF} 1/n[Cp_2ZrO]_n + R_2C{=}N^tBu \qquad (1)$$

oxo exchange reaction is relatively general, proceeding well with ketones, isocyanates, and ketenes. The proposed pathway for these reactions passes through an oxametallacyclobutane intermediate that is generated by overall [2 + 2] cycloaddition between the zirconocene imido fragment **2a** and the corresponding carbonyl substrate (Scheme 1). The imido/oxo exchange results

Scheme 1

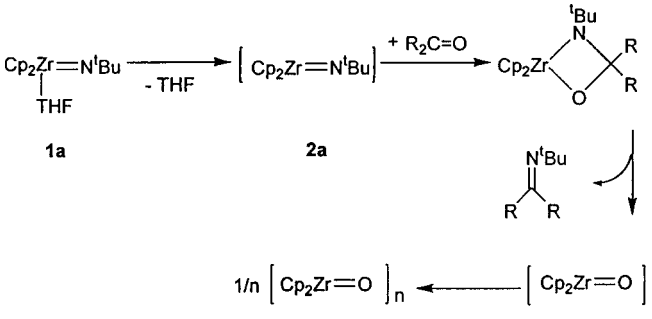

from the reversion of the zirconacycle to generate a zirconocene oxo species and the metathesized organic product which contains a new C=N group. The transient zirconium oxo complex oligiomerizes rapidly to $[Cp_2Zr{=}O]_n$. Extending the imido group transfer reaction to other C=X groups (X = S, N) would allow the use of readily available C=S or C=NR species (e.g., CS_2, RN=C=S, RN=C=NR) (eq 2). In the case where X = S, the

$$Cp_2(THF)Zr{=}N^tBu \;(\mathbf{1a}) + R_2C{=}X \xrightarrow{-\,THF} \text{"}Cp_2ZrX\text{"} + R_2C{=}N^tBu \qquad (2)$$

exchange reaction is also a form of desulfurization.[23−27] Finally, comparison of N/S and N/N exchange versus N/O exchange should provide a deeper understanding of the factors important in the overall group transfer reaction.

We report here an extension of the NR group transfer reaction of $Cp_2(THF)Zr{=}NR$ (**1a**−**c**) to CS_2, isothiocyanates, and symmetrical carbodiimides. The steric requirements in the cycloaddition reaction of **1a**−**c** with symmetrical carbodiimides and further reactivity of the diazametallacycles generated from the cycloaddition reactions of **1a**−**c** with carbodiimides were examined.

Results

Imido/Sulfur Exchange Reactions of $Cp_2(THF)Zr{=}N$-*t*-Bu (1a) with Organic Sulfur-Containing Heterocumulenes. Treatment of **1a** with CS_2 (1.5 equiv) at 25 °C resulted in the immediate formation of sulfido dimer **3** and *t*-BuN=C=S (73%) (eq 3). In the

$$Cp_2(THF)Zr{=}N^tBu \;(\mathbf{1a}) + S{=}C{=}S \xrightarrow{-\,THF} Cp_2Zr(\mu\text{-}S)_2ZrCp_2 \;(\mathbf{3}) + {}^tBuN{=}C{=}S \qquad (3)$$

crude reaction mixture, NMR integration versus an internal standard showed that sulfido dimer **3** formed in 95% yield. A smaller amount of the symmetrical carbodiimide *t*-BuN=C=N-*t*-Bu was also formed (10% yield). The ^1H NMR resonances and GC/MS of *t*-BuN=C=N-*t*-Bu and *t*-BuN=C=S were identical to those of authentic samples obtained from commercial suppliers. Sulfido dimer **3** was isolated as a green solid in 91% yield, and its identity was confirmed by comparison of MS and ^1H NMR spectroscopic data with literature values.[28]

To understand how *t*-BuN=C=N-*t*-Bu might have been formed in the reaction of CS_2 with **1a**, reactions of zirconocene imido complex **1a** with RN=C=S (R = *t*-Bu, Ph, Me) were carried out. Treatment of **1a** with *t*-BuN=C=S at 25 °C in C_6D_6 resulted in formation of sulfido dimer **3** in 88% yield and 1,3-di-*tert*-butylcarbodiimide

(19) Tóth, G.; Pintér, I.; Messmer, A. *Tetrahedron Lett.* **1974**, 735.
(20) McInnes, J. M.; Mountford, P. *Chem. Commun.* **1998**, 1669.
(21) McInnes, J. M.; Blake, A. J.; Mountford, P. *J. Chem. Soc., Dalton Trans.* **1998**, 3623.
(22) Lee, S. Y.; Bergman, R. G. *J. Am. Chem. Soc.* **1996**, *118*, 6396.
(23) Jones, W. D.; Chin, M. R.; Hoaglin, C. L. *Organometallics* **1999**, *18*, 1786.
(24) Jones, W. D.; Chin, R. M. *J. Am. Chem. Soc.* **1994**, *116*, 198.
(25) Curtis, M. D.; Druker, S. J. *J. Am. Chem. Soc.* **1997**, *119*, 1027.
(26) Vicic, D. A.; Jones, W. D. *J. Am. Chem. Soc.* **1999**, *121*, 7606.
(27) Vicic, D. A.; Jones, W. D. *Organometallics* **1997**, *116*, 11912.
(28) Bottomley, F.; Drummond, D.; Egharevba, G.; White, P. *Organometallics* **1986**, *5*, 1620.

in 92% yield calculated from ^{1}H NMR integration versus an internal standard (eq 4). We conclude that in the

$$Cp_2(THF)Zr{=}N^tBu \;(\mathbf{1a}) + {}^tBuN{=}C{=}S \xrightarrow{-\,THF} \mathbf{3} + {}^tBuN{=}C{=}N^tBu \qquad (4)$$

reaction of **1a** with CS_2, *t*-BuN═C═N-*t*-Bu is formed in a secondary reaction of **1a** with the initial product *t*-BuN═C═S. There was no evidence that *t*-BuN═C═N-*t*-Bu undergoes cycloaddition with unreacted **1a**.

Addition of phenyl isothiocyanate to **1a** in C_6D_6 gave an initial purple solution which turned green over 1 h. Analysis by ^{1}H NMR spectroscopy revealed two organometallic products, sulfido dimer **3** and another that was metastable. Over time, the metastable product was converted to **3** and 1-*tert*-butyl-3-phenylcarbodiimide (eq 5). The reaction was monitored at −30 °C, but no

$$Cp_2(THF)Zr{=}N^tBu \;(\mathbf{1a}) + PhN{=}C{=}S \xrightarrow{-\,THF} \mathbf{3} + {}^tBuN{=}C{=}NPh \qquad (5)$$

intermediate was identified at this temperature.

Monitoring the reaction of **1a** with methyl isothiocyanate at 25 °C by ^{1}H NMR spectroscopy showed the formation of sulfido dimer **3** and a second material tentatively identified as the metallacycle **4** based on its ^{1}H NMR resonances (eq 6). Heating the mixture at 96

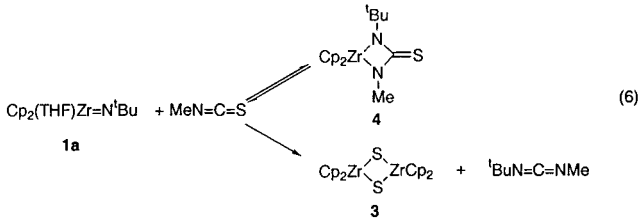

(6)

°C for 22 h led to nearly complete conversion of **4** to sulfido dimer **3** and CH_3N═C═N-*t*-Bu. Attempts to isolate metallacycle **4** in pure form were unsuccessful since it could not be prepared free of contamination from **3**.

Preparation of Sterically Hindered Zirconocene Imido Complexes. Results obtained from reaction of **1a** with isothiocyanates prompted us to examine the role of steric bulk at the nitrogen center in the reactions of zirconocene imido complexes with small heterocumulenes. To achieve this, we generated arylimido complexes with large alkyl substituents in the ortho positions of the phenyl ring. The zirconocene imido complex $Cp_2(THF)Zr{=}N$-2,6- *i*-$Pr_2C_6H_3$ (**1b**) was isolated in 80% yield from thermolysis of the methyl amide **5a** in THF (eq 7). Triangular, orange crystals suitable for X-ray

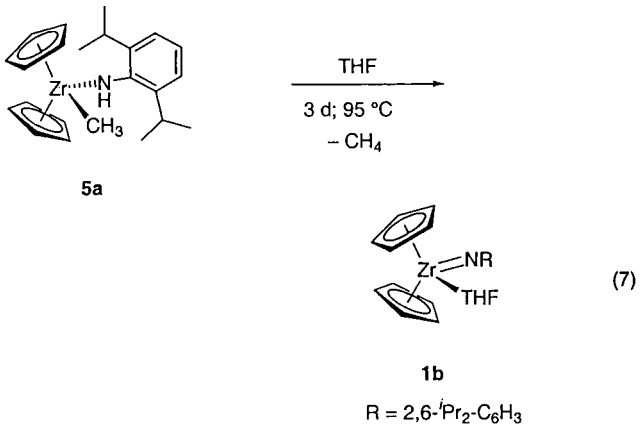

(7)

analysis were obtained from the slow diffusion of hexanes into a toluene solution at −35 °C. The ORTEP diagram of complex **1b** is shown in Figure 1. The Zr−N bond distance in **1b** was found to be 1.888(2) Å, 0.06 Å longer than the Zr−N distance in **1a** (1.826(4) Å)[29] (Table 1; see Table 2 for crystallographic data on **1b**). In addition, the imido linkage in **1b** (∠Zr−N−C = 159°) deviates more strongly from linearity than the corresponding bond in the analogue **1a** (174.4(3)°). Both of these structural features imply a slightly lower Zr−N bond order in **1b** than **1a**. This finding may be the result of both electronic and steric factors that reduce the extent of π-donation from the imido lone pair to the empty metal-centered b_2 antibonding orbital.[30] The Zr−O bond distance to the THF ligand was found to be 2.261(2) Å, 0.02 Å longer than the Zr−O bond distance in **1a** (2.240(4) Å).[29]

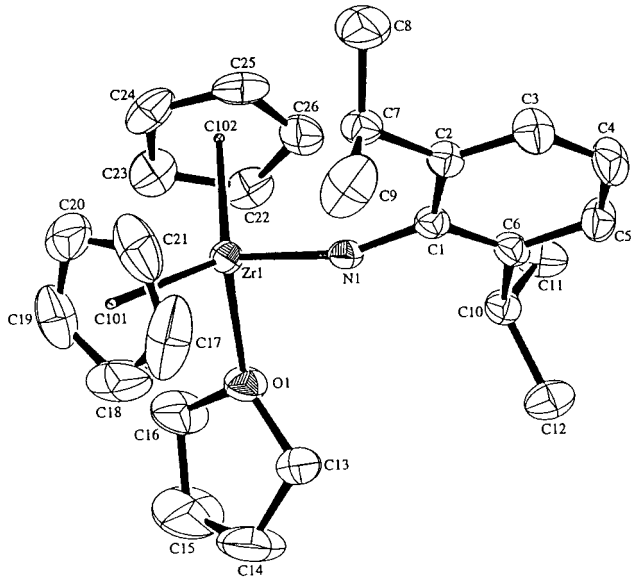

Figure 1. ORTEP diagram of **1b**. The thermal ellipsoids are scaled to represent the 50% probability surface.

Table 1. Selected Bond Lengths (Å) and Bond Angles (deg) for Compound 1b

Bond Lengths			
Zr1−O1	2.261(2)	Zr1−N1	1.888(2)
Zr1−C101	2.312(1)	Zr1−C102	2.277(1)
N1−C1	1.368(3)	C1−C2	1.435(3)
C1−C6	1.430(4)	C7−C8	1.510(4)
C2−C7	1.523(4)	C6−C10	1.525(4)
Bond Angles			
O1−Zr1−N1	97.94(8)	O1−Zr1−C101	101.50(6)
O1−Zr1−C102	104.61(5)	N1−Zr1−C101	113.69(6)
N1−Zr1−C102	107.07(6)	C101−Zr1−C102	127.22(1)
Zr1−O1−C13	124.5(2)	Zr1−O1−C16	123.4(2)
C13−O1−C16	107.9(2)	Zr1−N1−C1	159.1(2)
N1−C1−C2	121.4(2)	N1−C1−C6	121.1(2)

(29) Walsh, P. J.; Hollander, F. J.; Bergman, R. G. *Organometallics* **1993**, *12*, 3705.
(30) Green, J. C. *Chem. Soc. Rev.* **1998**, *27*, 263.

Table 2. Crystallographic Data for Compounds 1b and 6

	1b	6
empirical formula	$C_{26}H_{35}NOZr$	$C_{28}H_{39}NZr$
fw	468.29	480.82
cryst color, habit	orange, triangular	orange, block
cryst dimens	0.42 × 0.36 × 0.22 mm	0.08 × 0.27 × 0.45 mm
cryst syst	orthorhombic	monoclinic
lattice type	primitive	primitive
lattice params	a = 15.2427(1) Å	a = 17.2829(2) Å
	b = 9.3678(1) Å	b = 8.8432(2) Å
	c = 16.5042(2) Å	c = 17.1648(3) Å
	β = 120.00°	β = 106.308(1)°
	V = 2356.64(3) Å^3	V = 2517.85(7) Å^3
space group	$Pca2_1$ (#29)	$P2_1/c$ (#14)
Z value	4	4
D_{calc}	1.321 g/cm^3	1.268 g/cm^3
F_{000}	880.00	976.00
μ(Mo Kα)	4.82 cm^{-1}	4.49 cm^{-1}
diffractometer	SMART CCD	SMART CCD
radiation	Mo Kα (λ = 0.71069 Å) graphite monochromated	Mo Kα (λ = 0.71069 Å) graphite monochromated
detector position	60.00 mm	60.00 mm
temperature	−112 °C	−106 °C
scan type	ω (0.30 deg/frame)	ω (0.30 deg/frame)
scan rate	10.0 s/frame	10.0 s/frame
$2\theta_{max}$	51.9°	52.2°
no. of reflns measured	total: 11 277	total: 11 871
	unique: 4372 (R_{int} = 0.032)	unique: 4744 (R_{int} = 0.029)
corrections	Lorentz−polarization absorption (T_{max} = 0.93 T_{min} = 0.82)	Lorentz−polarization absorption (T_{max} = 0.93 T_{min} = 0.73)
structure solution	direct methods (SIR92)	direct methods (SIR92)
refinement	full-matrix least-squares	full-matrix least-squares
p-factor	0.030	0.030
anomalous dispersion	all non-hydrogen atoms	all non-hydrogen atoms
no. observations (I>3.00σ(I))	3687	3118
no. variables	261	271
reflection/param ratio	14.13	11.51
residuals: R; R_w; R_{all}	0.024; 0.033; 0.027	0.027; 0.031; 0.049
goodness of fit indicator	1.35	1.13
max shift/error in final cycle	0.00	0.00
max peak in final diff map	0.27 e$^-$/Å^3	0.35 e$^-$/Å^3
min peak in final diff map	−0.41 e$^-$/Å^3	−0.49 e$^-$/Å^3

An attempt to prepare an imido complex that is even more sterically congested than $Cp_2(THF)Zr{=}N$-2,6-i-$Pr_2C_6H_3$ was made by replacing the i-Pr substituents in the ortho positions of the aromatic ring with t-Bu groups. Methyl amide **5b** was prepared in a procedure analogous to the one used for the i-Pr analogue (Scheme 2). Treatment of $Cp_2Zr(Me)(Cl)$ with 1 equiv of LiNH-2,4,6-t-$Bu_3C_6H_2$ cleanly afforded **5b** in 61% yield. Several differences were noted during heating of compound **5b**, compared with the thermolysis reaction of other analogues. For example, methyl amide complex **5a** is cleanly converted to the zirconocene imido complex **1b** upon heating at 95 °C for 3 days. In contrast, heating complex **5b** at 95 °C showed >95% unreacted amide after 1 day. At 135 °C, a new product was cleanly formed over the course of 5 days. The ^{1}H NMR spectrum of this material revealed a new NH resonance (δ 6.61) and only two intact nine-hydrogen t-Bu signals at δ 1.42 and 1.37. A third aliphatic methyl singlet was observed at δ 1.65 integrating to six hydrogens. Recrystallization of the isolated product from Et_2O at −35 °C gave orange block crystals. Analysis by X-ray diffraction was performed, and the ORTEP diagram is presented in Figure 2. This shows that the product is the six-membered cyclometalated complex **6** (Scheme 2) instead of the desired zirconocene imido complex. The six-membered metallacycle ring adopts an unusual "boat" conformation. The dihedral angle between the plane defined by Zr(1), N(1), C(1), and C(2) and the plane defined by N(1), C(2), C(3), and C(10) is 55° (Table 3; see Table 2 for crystallographic data of **6**). The hydrogen attached to N(1), H(1), was located in a plane formed by Zr(1), C(10), and N(1). Its position was fixed to correspond to sp^2 hybrid-

Scheme 2

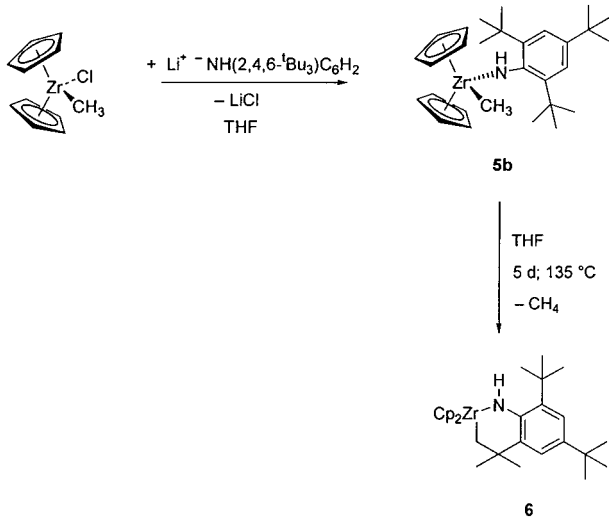

(31) Cardin, D. J.; Lappert, M. F.; Raston, C. L. *Chemistry of Organo-Zirconium and -Hafnium Compounds*; Ellis Horwood: New York, 1986.

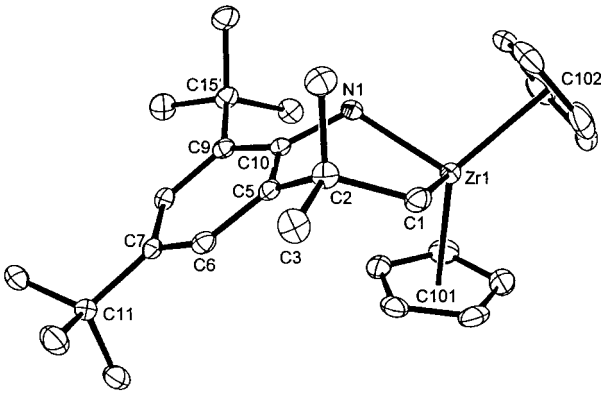

Figure 2. ORTEP diagram of **6**. The thermal ellipsoids are scaled to represent the 50% probability surface.

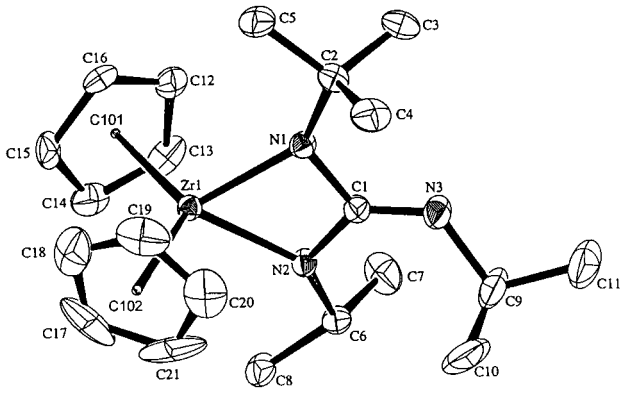

Figure 3. ORTEP diagram of **7a**. The thermal ellipsoids are scaled to represent the 50% probability surface.

Table 3. Selected Bond Lengths (Å) and Bond Angles (deg) for Compound 6

	Bond Lengths		
Zr1−N1	2.075(2)	Zr1−C1	2.294(3)
N1−C10	1.418(3)	C1−C2	1.568(4)
C9−C15	1.547(4)	C2−C4	1.536(4)
C2−C3	1.537(4)	C7−C11	1.543(4)
C2−C5	1.549(3)	C9−C10	1.423(3)
C5−C10	1.416(3)	C5−C6	1.392(3)
Zr1−C101	2.2458(2)	Zr1−C102	2.2333(2)
	Bond Angles		
N1−Zr1−C1	87.05(8)	Zr1−C1−C2	112.7(2)
Zr1−N1−C10	117.8(2)	C1−C2−C4	109.8(2)
C1−C2−C3	107.0(2)	C3−C2−C4	105.8(2)
C1−C2−C5	114.3(2)	N1−C10−C5	116.7(2)
C2−C5−C6	120.5(2)	N1−C10−C9	123.5(2)
C6−C5−C10	118.1(2)	C6−C7−C11	121.6(2)
N1−C10−C9	123.5(2)	C101−Zr1−C102	130.68(1)
N1−Zr1−C102	105.90(6)	C1−Zr1−C101	113.02
C1−Zr1−C102	107.48(7)	N1−Zr1−C101	113.0.02

ization on N(1). The Zr−N bond distance was found to be 2.075(2) Å, which is typical for zirconocene amido complexes.[29,31]

Reactions of 1a with Symmetrical Carbodiimides. A variety of carbodiimides were added to **1a** to further probe the influence of steric hindrance in the formal [2 + 2] cycloaddition reaction and to examine the possibility of imido group metathesis. The results are summarized in Table 4. Reaction with 1,3-diisopropylcarbodiimide in C_6H_6 generated a purple solution. The resulting purple solid, isolated after the removal of solvent under reduced pressure, was crystallized by slow evaporation of a hexanes solution in 97% yield. An ORTEP diagram obtained from X-ray diffraction studies (Figure 3) showed the complex to have structure **7a**. The metallacyclobutane ring deviates slightly from planarity; the dihedral angle between the plane formed by Zr(1), N(1), and N(2) and the plane formed by C(1), N(1), and N(2) is 168° (Table 5; see Table 6 for crystallographic data). The N1−C1 and N2−C1 bond distances of 1.411(4) and 1.415(4) Å, respectively, are significantly longer than the N3−C1 bond distance of 1.280(4) Å. The shorter N3−C1 bond distance supports a high degree of double-bond character in the exocyclic position of the ring and more single-bond character between N1−C1 and N2−C1. These findings indicate that the first resonance structure drawn in Figure 4 is the predominant form for **7a**, with smaller contributions from the other two resonance structures shown. The predominant single-bond character of N1−C1 and N2−C1 is further supported by comparison of its N−C bond distances with those of a previously reported diazametallacycle, **8** (1.472(6) and 1.481(5) Å; Figure 5).[13,14] The solid-state structure of **7a** shows the isopropyl substituent on the exocyclic nitrogen pointing toward the N2 isopropyl group. We believe that this geometry is preferred in order to reduce steric interaction between the N3 isopropyl group and the *t*-Bu group on N1.

Table 4. Reaction of Zirconocene Imido Complexes 1a−c with Symmetrical Carbodiimides

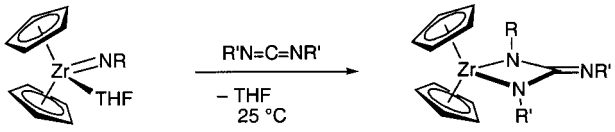

1a-c **7, 9, 11**

carbodiimides	$Cp_2(THF)Zr{=}Nt\text{-}Bu$ (**1a**)	$Cp_2(THF)Zr{=}N(2,6\text{-}i\text{-}Pr_2)Ph$ (**1a**)	$Cp_2(THF)Zr{=}N(2,6\text{-}Me_2)Ph$ (**1a**)
R′ = *i*-Pr	purple crystals 97% yield; **7a**	purple crystals 82% yield; **9a**	purple crystals 92% yield; **11a**
R′ = cyclohexyl	purple crystals 81% yield; **7b**	purple crystals 72% yield; **9b**	purple crystals 88% yield; **11b**
R′ = *p*-tolyl	blue crystals 81% yield; **7c**	purple solution not isolated; **9c**	magenta crystals 89% yield; **11c**
R′ = $SiMe_3$	red crystals 45% yield; **7d**	no reaction[b]	red crystals 73% yield; **11d**
R′ = ^{t}Bu	no reaction[a]	no reaction[b]	purple crystals 87% yield; **11e**

[a] No reaction was observed at 85 °C. [b] No reaction was observed at 120 °C.

Table 5. Selected Bond Lengths (Å) and Bond Angles (deg) for Compound 7a

	Bond Lengths		
Zr1−N1	2.088(2)	Zr1−N2	2.091(2)
Zr1−C101	2.2501(3)	Zr1−C102	2.2644(3)
N1−C1	1.411(4)	N1−C2	1.480(3)
N2−C1	1.415(4)	N2−C6	1.476(4)
N3−C1	1.280(4)	N3−C9	1.483(4)
	Bond Angles		
N1−Zr1−N2	65.33(8)	N1−Zr1−C101	111.82(8)
N1−Zr1−C102	112.61(8)	N2−Zr1−C101	113.74(6)
N2−Zr1−C102	109.18(6)	C101−Zr1−C102	127.550(10)
Zr1−N1−C1	93.8(2)	Zr1−N1−C2	141.2(2)
C1−N1−C2	122.8(2)	Zr1−N2−C1	93.6(2)
Zr1−N2−C6	142.0(2)	C1−N2−C6	123.4(2)
C1−N3−C9	123.2(3)	N1−C1−N2	105.9(2)
N1−C1−N3	121.3(3)	N2−C1−N3	132.7(3)
N1−C2−C3	110.1(2)	N1−C2−C4	112.3(3)
N1−C2−C5	107.0(2)	N2−C6−C8	108.1(2)
N2−C6−C7	112.3(3)	N3−C9−C11	108.2(3)
N3−C9−C10	109.5(3)		

Complex **1a** was next treated with 1 equiv of 1,3-dicyclohexylcarbodiimide (CycN═C═NCyc). This resulted in an immediate color change from yellow to purple. Complex **7b** was isolated as analytically pure crystals in 81% yield by storing a hexanes solution at −35 °C for 1 day. The ^{13}C NMR spectrum of this material in C_6D_6 displayed a resonance at 138 ppm that is characteristic of the C═N functionality for this class of zirconacycles. An IR stretch at 1583 cm^{-1} supports the presence of a C═N moiety in the molecule as well.

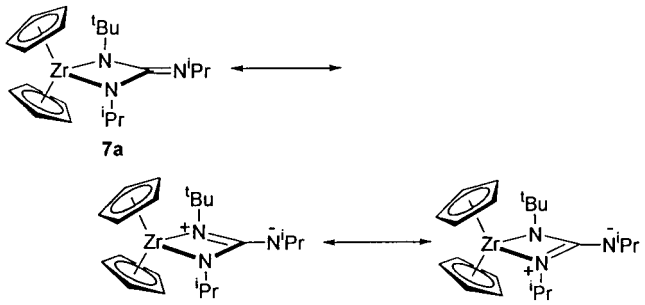

Figure 4. Resonance structures for diazametallacycle complex **7a**.

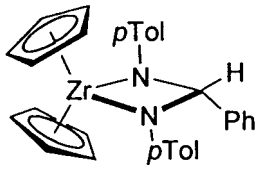

8

Figure 5. Diazametallacycle complex **8**.

The related diazametallacycles **7c** and **7d** (Table 4) were prepared from **1a** and 1,3-di-*p*-tolylcarbodiimide and bis-1,3-trimethylsilylcarbodiimide, respectively. However, treatment of **1a** with 1,3-di-*tert*-butylcarbodiimide in C_6D_6 gave no reaction even upon heating (85 °C, 2 h).

Table 6. Crystallographic Data for Compounds 7a and 9a

	7a	**9a**
empirical formula	$C_{21}H_{33}N_3Zr$	$C_{29}H_{41}N_3Zr$
fw	418.73	522.88
cryst color, habit	red-orange, block	red, plate
cryst dimens	0.18 × 0.20 × 0.20 mm	0.08 × 0.27 × 0.45 mm
cryst syst	orthorhombic	monoclinic
lattice type	primitive	primitive
lattice params	a = 9.2244(2) Å	a = 10.0525(1) Å
	b = 12.2751(3) Å	b = 15.6492(2) Å
	c = 18.7973(4) Å	c = 17.3805(2) Å
	β = 120.00°	97.268(1)°
	V = 2128.43(7) Å^3	V = 2712.22(5) Å^3
space group	$P2_12_12_1$ (#19)	$P2_1/n$ (#14)
Z value	4	4
D_{calc}	1.335 g/cm^3	1.280 g/cm^3
F_{000}	880.00	1104.00
μ(Mo Kα)	5.24 cm^{-1}	4.26 cm^{-1}
diffractometer	SMART CCD	SMART CCD
radiation	Mo Kα (λ = 0.71069 Å)	Mo Kα (λ = 0.71069 Å)
	graphite monochromated	graphite monochromated
detector position	60.00 mm	60.00 mm
temperature	−152 °C	−125 °C
scan type	ω (0.30 deg/frame)	ω (0.30 deg/frame)
scan rate	10.0 s/frame	10.0 s/frame
$2\theta_{max}$	52.3°	52.1°
no. of reflns measured	total: 7952	total: 12 691
	unique: 3700 (R_{int} = 0.026)	unique: 4944 (R_{int} = 0.031)
corrections	Lorentz-polarization absorption	Lorentz-polarization absorption
	(T_{max} = 0.93 T_{min} = 0.82)	(T_{max} = 0.90 T_{min} = 0.81)
structure solution	direct methods (SIR92)	direct methods (SIR92)
refinement	full-matrix least-squares	full-matrix least-squares
p-factor	0.030	0.030
anomalous dispersion	all non-hydrogen atoms	all non-hydrogen atoms
no. observations (I>3.00σ(I))	3287	3572
no. variables	226	298
reflection/param ratio	14.54	11.99
residuals: R; R_w; R_{all}	0.026; 0.036; 0.031	0.035; 0.049; 0.050
goodness of fit indicator	1.46	1.81
max shift/error in final cycle	0.00	0.00
max peak in final diff map	0.35 e$^-$/Å^3	0.49 e$^-$/Å^3
min peak in final diff map	−0.36 e$^-$/Å^3	−0.47 e$^-$/Å^3

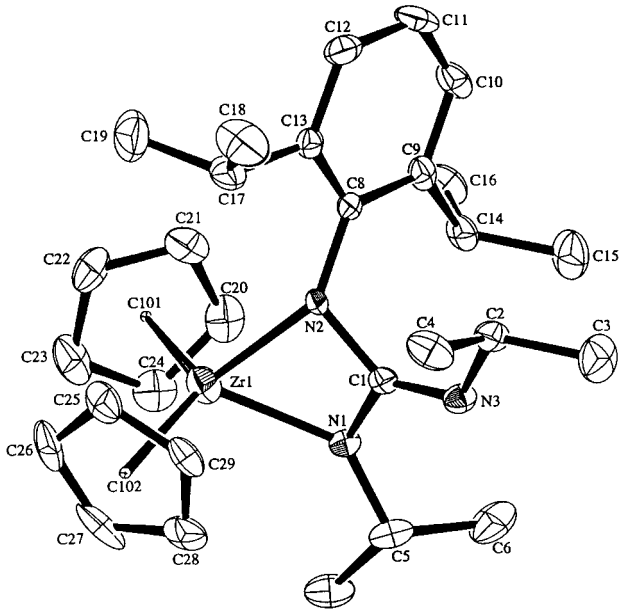

Figure 6. ORTEP diagram of **9a**. The thermal ellipsoids are scaled to represent the 50% probability surface.

Table 7. Selected Bond Lengths (Å) and Bond Angles (deg) for Compound 9a

	Bond Lengths		
Zr1−N1	2.121(3)	Zr1−N2	2.109(3)
Zr1−C101	3.2354(3)	Zr1−C102	2.2509(3)
N1−C1	1.393(4)	N1−C5	1.449(4)
N2−C1	1.441(4)	N2−C8	1.423(4)
N3−C1	1.275(4)	N3−C2	1.463(4)
	Bond Angles		
N1−Zr1−N2	64.8(1)	N1−Zr1−C101	114.39(7)
N1−Zr1−C102	107.62(8)	N2−Zr1−C101	110.53(7)
N2−Zr1−C102	113.32(7)	C101−Zr1−C102	128.65(1)
Zr1−N1−C1	92.5(2)	Zr1−N1−C5	139.6(2)
C1−N1−C5	120.6(3)	Zr1−N2−C8	141.1(2)
C1−N2−C8	121.2(3)	C1−N3−C2	121.4(3)
N1−C1−N2	106.2(3)	N1−C1−N3	123.2(3)
N2−C1−N3	130.4(3)	N3−C2−C3	108.1(3)
N3−C2−C3	110.8(3)	N1−C5−C7	109.1(3)
N1−C5−C6	112.1(3)	N2−C8−C9	120.6(3)
N2−C8−C13	120.3(3)		

Reactions of 1b and 1c with Carbodiimides. Reaction of the hindered arylimido complex **1b** with 1 equiv of *i*-PrN═C═N-*i*-Pr yielded **9a** cleanly in 97% isolated yield (Table 4). Purple X-ray quality crystals were obtained by slow evaporation of a solution of diazametallacycle **9a** in hexanes (82% yield). An ORTEP diagram of **9a** is shown in Figure 6. In contrast to the four-membered zirconacycle **7a**, the metallacyclobutane ring is not planar. The dihedral angle between the plane formed by Zr(1), N(1), and N(2) and the plane formed by C(1), N(1), and N(2) is 156° (Table 7). This deviation from planarity is attributed to the congestion introduced by the *i*-Pr groups on the aromatic ring. The bond distances N1−C1 and N2−C1 are 1.393(4) and 1.441(4) Å, respectively. The N3−C1 bond distance of 1.275(4) Å is consistent with lack of complete delocalization within the ligand and greater electron density between N3 and C1.

Complex **1b** also reacts with CycN═C═NCyc cleanly to afford one product by ^{1}H NMR spectroscopy. The isolated purple solid was crystallized from hexanes in 72% yield to afford diazametallacycle **9b**, which has been fully characterized (Table 4).

When **1b** was treated with 1,3-di-*p*-tolylcarbodiimide for 4 days at 45 °C in C_6D_6, the solution turned brown and a new metallacycle formed whose structure is tentatively assigned as the unsymmetrical metallacycle **9c**. The ^{1}H NMR spectrum shows one peak in the cyclopentadienyl region (δ 6.0, 10 H's). There are two resonances at δ 2.15 and 2.08, each integrating to 3 H's that are tentatively assigned as those due to the endocyclic and exocyclic aromatic methyl groups. Additionally, there are two different *i*-Pr signals at δ 1.46 and 1.23, indicating steric crowding of the substituted aryl moiety on nitrogen. Heating the unsymmetrical metallacycle at 75 °C for 15 h resulted in a color change from brown to purple, and spectroscopic analysis revealed the apparent conversion to a new rearranged product **10** (eq 8). This is evident in the ^{1}H NMR

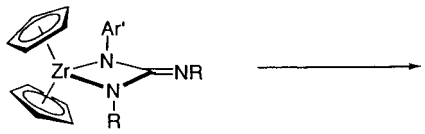

9a

Ar' = 2,6-^{i}Pr$_2$-C$_6$H$_3$
R = *p*-tolyl

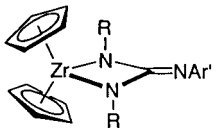

10 (8)

spectrum, which reveals a new chemical shift for the cyclopentadienyl ligands (δ 5.96). The methyl groups on the tolyl rings are now spectroscopically equivalent with a chemical shift at δ 2.15 integrating to six hydrogens. The *i*-Pr groups on the nitrogen-containing aromatic ring are also equivalent with the methyl signals observed as one doublet (δ 1.44, d, J = 6 Hz) and the methine proton signal appearing at 3.75 ppm. Unlike **9c**, heating diazametallacycles **9a** and **9b** to 105 °C did not induce an analogous rearrangement.

Treatment of the more sterically congested zirconocene imido complex **1b** with either *t*-BuN═C═N-*t*-Bu or Me_3SiN═C═N$SiMe_3$ gave no reaction at 25 °C or on heating to 120 °C.

Zirconocene imido complex **1c** was found to undergo similar reactions with symmetrical carbodiimides, RN═C═NR (R = *i*-Pr, cyclohexyl, *p*-tolyl, $SiMe_3$, and *t*-Bu). The reactions were carried out by treating **1c** with 1 equiv of the corresponding carbodiimide at 25 °C in C_6H_6. In all cases examined, clean conversion to a new metallacycle was observed by ^{1}H NMR spectroscopy, and these complexes were crystallized to give good yields (>70%) of the zirconacycle products **11a**−**d** (Table 4).

Stoichiometric Carbodiimide Metathesis. We wanted to pursue imido group metathesis reactions between isolated diazametallacycle complexes and carbodiimides as a method for generating new zirconium-containing metallacycles and unsymmetrical carbodiimides. When metallacycle **7d** was heated at 85 °C in the presence of 10 equiv of Me_3SiN═C═N$SiMe_3$, the reaction mixture turned from red to pale yellow. Examination by ^{1}H NMR spectroscopy revealed that the

Scheme 3

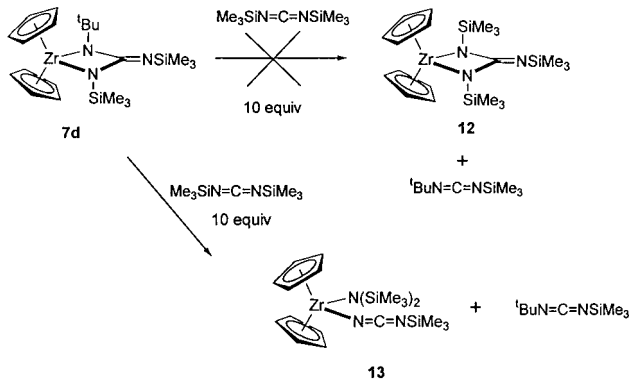

anticipated symmetrical diazametallacycle **12** (Scheme 3) was not the product generated under these conditions. Instead of the two Me_3Si singlets that would be expected if **12** had formed, we observed three singlets (all integrating to 9 H) at δ 0.39, 0.30, and 0.20. Isolation of a light yellow solid followed by recrystallization from hexanes at −35 °C afforded yellow blocks in 85% yield. X-ray analysis established the identity of this complex as the amide species **13** (Scheme 3) resulting from an overall Me_3Si group transfer from N1 to the nitrogen-labeled N3 in the ORTEP diagram (Figure 7). The chain

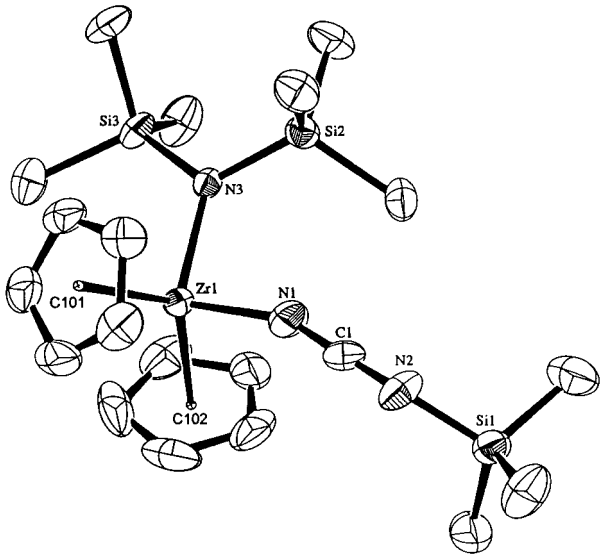

Figure 7. ORTEP diagram of **13**. The thermal ellipsoids are scaled to represent the 50% probability surface.

of atoms Zr(1)−N(1)−N(2)−Si(1) is not linear (Table 8; see Table 9 for crystallographic data). The NCN($SiMe_3$) ligand coordinates to Zr(1) with a Zr(1)−N(1)−C(1) bond angle of 158°. Within the NCN($SiMe_3$) ligand, the N(1)−C(1)−N(2) bond angle is 176°, but the terminal $SiMe_3$ is quite bent; the value of the C(1)−N(2)−Si(1) bond angle is 137°. The dihedral angle between the least-squares plane defined by Zr(1), N(1), C(1), and N(2) and the plane defined by N(1), C(1), N(2), and Si(1) is 77.8°.

The bond lengths for N3−Si2, N3−Si3, and N2−Si1 in **13** were found to be 1.749(3), 1.736(3), and 1.717(3) Å, respectively. These values are similar to the reported N−Si bond lengths in a zirconium dialkyl bis[bis-(trimethylsilyl)amido] complex (ca. 1.7 Å).[31] The Zr−N1 bond distance (2.086(3) Å) is typical for bond

Table 8. Selected Bond Lengths (Å) and Bond Angles (deg) for Compound 13

Bond Lengths			
Zr1−N1	2.086(3)	Zr1−N3	2.142(3)
Zr1−C101	2.2530(3)	Zr1−C102	2.2495(3)
Si1−N2	1.717(3)	Si1−C2	1.834(5)
Si1−C3	1.817(5)	N2−C1	1.227(5)
Si2−N3	1.749(3)	Si2−C9	1.884(4)
Si2−C6	1.873(4)	Si3−C9	1.871(4)
Si3−N3	1.736(3)	N1−C1	1.190(5)
Bond Angles			
N1−Zr1−N3	99.9(1)	N1−Zr1−C101	103.05(9)
N1−Zr1−C102	100.64(10)	N3−Zr1−C101	108.56(7)
N3−Zr1−C102	110.54(7)	C101−Zr1−C102	129.33(1)
N2−Si1−C2	110.2(2)	N2−Si1−C3	106.3(2)
N2−Si1−C4	109.0(2)	N3−Si2−C6	115.0(2)
C2−Si1−C4	109.8(2)	N3−Si3−C9	112.3(2)
N3−Si2−C5	113.8(2)	Si1−N2−C1	136.9(3)
N3−Si3−C10	115.3(2)	Zr1−N3−Si3	123.4(1)
C8−Si3−C10	103.8(2)	N1−C1−N2	176.5(4)
Zr1−N1−C1	158.4(3)	Si2−N3−Si3	117.3(2)
Zr1−N3−Si2	119.0(1)		

Table 9. Crystallographic Data for Compound 13

empirical formula	$C_{20}H_{37}N_3Si_3Zr$
fw	495.01
cryst color, habit	yellow, block
cryst dimens	0.34 × 0.24 × 0.12 mm
cryst syst	orthorhombic
lattice type	primitive
lattice params	a = 9.3868(4) Å
	b = 20.5709(9) Å
	c = 26.245(1) Å
	β = 90.00°
	V = 5067.7(3) Å^3
space group	*Pbca* (#61)
Z value	4
D_{calc}	1.297 g/cm^3
F_{000}	2080.00
μ(Mo Kα)	5.86 cm^{-1}
diffractometer	SMART CCD
radiation	Mo Kα (λ = 0.71069 Å) graphite monochromated
detector position	60.00 mm
temperature	−98.0 °C
scan type	ω (0.30 deg/frame)
scan rate	10.0 s/frame
$2\theta_{max}$	52.2°
no. of reflns measured	total: 23812
	unique: 5190 (R_{int} = 0.042)
corrections	Lorentz−polarization absorption (T_{max} = 0.87 T_{min} = 0.79)
structure solution	direct methods (SIR92)
refinement	full-matrix least-squares
p-factor	0.030
anomalous dispersion	all non-hydrogen atoms
no. observations (I>3.00σ(I))	3087
no. variables	244
reflection/param ratio	12.65
residuals: R; R_w; R_{all}	0.031; 0.039; 0.055
goodness of fit indicator	1.36
max shift/error in final cycle	0.00
max peak in final diff map	0.46 e$^-$/Å^3
min peak in final diff map	−0.44 e$^-$/Å^3

distances seen in several zirconocene amido complexes. However, the Zr−N3 bond distance (2.142(3) Å) is slightly longer than normal, probably because of steric crowding around the metal center. This seems to be a reasonable explanation since there are three resonances in the ^{1}H NMR spectrum for the Me_3Si groups, indicating that free rotation is inhibited at ambient temperature due to steric congestion. The N1−C1 bond distance is 1.190(5) Å and the N2−C1 bond distance is 1.227(5) Å, which clearly demonstrates substantial double bond

character between these atoms, with greater electron density in the N1−C1 bond than the N2−C1 bond.

Since trimethylsilyl migration to generate **13** was observed when **7d** was treated with excess $Me_3SiN{=}C{=}NSiMe_3$, we tried to prepare a symmetrical metallacycle from a different starting zirconacycle. When complex **7a** was treated with 2 equiv of *i*-PrN=C=N-*i*-Pr in C_6H_6 at 25 °C over ca. 1 h, the solution remained purple in color, but analysis by ^{1}H NMR spectroscopy gave good indication that we indeed had generated a symmetrical metallacycle **14** with the concurrent extrusion of *i*-PrN=C=N-*t*-Bu (eq 9). Storing a hexane

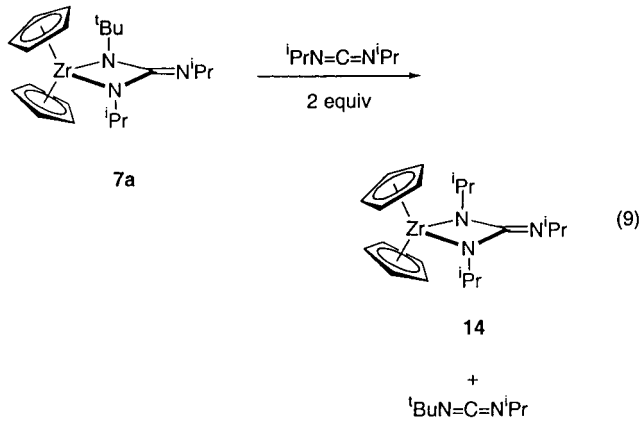

(9)

solution at −35 °C for 2 days gave purple needles of compound **14** in 86% isolated yield. The ^{1}H NMR spectrum of this compound at 25 °C showed one cyclopentadienyl resonance at δ 6.01, a multiplet at δ 4.5 (exocyclic methine), a multiplet at δ 4.2 integrating to two protons (endocyclic methines), and a doublet at δ 1.4 integrating to six hydrogens (exocyclic *i*-Pr methyl groups). However, a broad resonance for the two endocyclic *i*-Pr methyl groups was observed at ca. δ 1.0, integrating to 12 protons. A variable-temperature NMR experiment (−20 to 80 °C) revealed that complex **14** exhibits fluxional behavior with a coalescence temperature of 46 °C and a $\Delta G^{\ddagger}$ of 15.3 *k*cal/mol. A stack plot showing this fluxionality is presented in Figure 8.

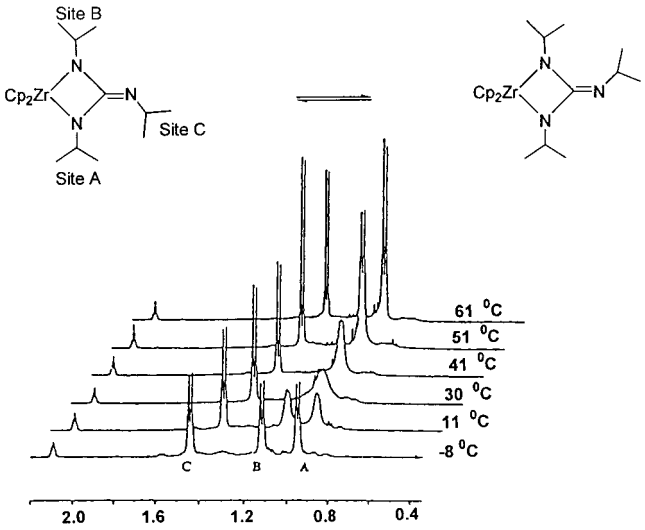

Figure 8. Stack plot illustrating the fluxional behavior exhibited by complex **14**.

Discussion

The initial formation of heterometallacyclobutanes is proposed for essentially all of the reactions that we have observed between imido complexes and heterocumulenes. Besides providing an efficient explanation for the observed results, metallacycle intermediates have been observed or proposed in many previously reported reactions of imido complex **1a**.

Imido Group Transfer: Reaction with CS_2. The reaction of CS_2 with *N*-*tert*-butylimidozirconocene **1a** yields bridging sulfido complex **3** and a mixture of *t*-BuN=C=S and *t*-BuN=C=N-*t*-Bu. The most likely mechanism for this transformation involves cycloaddition of CS_2 to imido complex **1a**, yielding a thiaazametallacyclobutane intermediate **18** (Scheme 4). Complex

Scheme 4

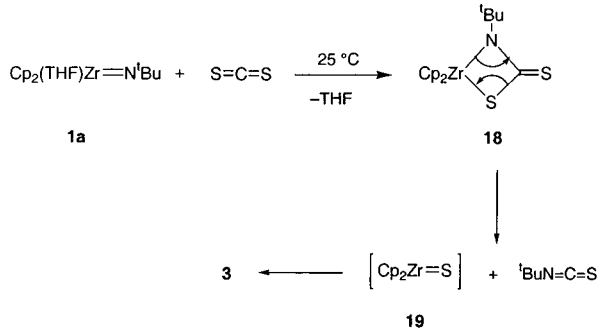

18 may undergo cycloreversion to give *t*-BuN=C=S and the sulfido complex **19** (which dimerizes). The carbodiimide is proposed to form from an overall [2 + 2] cycloaddition reaction between *t*-BuN=C=S and **1a** to afford thiaazametallaycle **20** (Scheme 5). Reversion of

Scheme 5

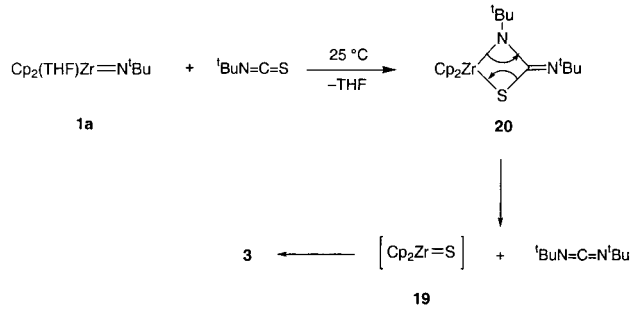

this metallacycle would generate zirconocene sulfido complex **19** with the concurrent extrusion of *t*-BuN=C=N-*t*-Bu.

Imido Group Transfer: Reaction with *t*-BuN=C=S. To test the hypothesis of isothiocyanate generation in the CS_2 reaction and further explore heterocumulene cycloaddition with **1a**, we carried out the direct reaction of the imido complex with *t*-BuN=C=S and other isothiocyanates. As predicted in Scheme 5, this led to carbodiimides (*t*-BuN=C=NR), consistent with the production of *t*-BuN=C=N-*t*-Bu in the reaction of CS_2 with **1a**.

In principle, the reaction may produce two initial metallacycles, **21** or **22** (Figure 9). With phenyl- and *tert*-butyl isothiocyanate, only one metallacycle is observed. However, with methyl isothiocyanate, two species are

21 22

Figure 9. Two possible regioisomers, **21** and **22**.

formed, the sulfido dimer **3** and the tentatively assigned metallacycle **4**. With heating, **4** reverts to the imido complex **1a** and the isothiocyanate and is eventually converted to **3** (eq 6). We assume that the formation of a metallacycle of type **22** only in the case R = Me is the result of the smaller steric interaction of the incoming methyl group with the Cp_2Zr coordination sphere.

Steric Influence of the Zirconocene Imido Fragment. Previous work from our laboratories demonstrated that there is a strong steric effect in the cycloaddition reaction between zirconocene imido complexes **1b**,**c** and alkynes (Scheme 6).[32,33] Increasing the

Scheme 6

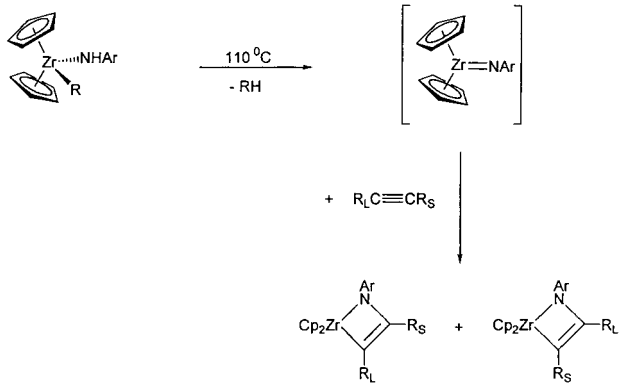

size of either the N-aryl group or the α-substituent on the alkyne enhances the thermodynamic regioselectivity of metallacycle formation. It was observed that the larger alkyl group on the unsymmetrical alkyne is located α to the zirconium metal center in the metallacycles.[32,33]

To examine this effect in heterocumulene cycloadditions, we wanted to utilize sterically encumbered zirconocene imido complexes. In our current work, we were able to isolate the zirconocene imido complex Cp_2(THF)Zr=N(2,6-*i*-$Pr_2C_6H_3$) (**1b**) from thermolysis of the methyl amide **5a** in THF (eq 7). However, attempts to generate imido complexes with the larger N-2,4,6-*t*-$Bu_3C_6H_2$ substituent proved unsuccessful due to cyclometalation of one of the *t*-Bu groups of the anilide to afford **6** (Scheme 2). We could not discern from the spectroscopic data if the desired zirconocene imido complex formed initially, followed by subsequent deprotonation of the *t*-Bu moiety by the imide nitrogen, or if **6** was generated directly from methyl amide **5b**, with concurrent loss of methane. Inter- and intramolecular carbon−hydrogen bond activations have been observed in other early metal monomeric imido systems,[34−36] but this appears to be a rare observation of the addition of an unactivated aliphatic C−H bond across a zirconocene M=N linkage.

(32) Walsh, P. J.; Baranger, A. M.; Bergman, R. G. *J. Am. Chem. Soc.* **1992**, *114*, 1708−1719.
(33) Walsh, P. J.; Hollander, F. J.; Bergman, R. G. *J. Am. Chem. Soc.* **1988**, *110*, 8729.

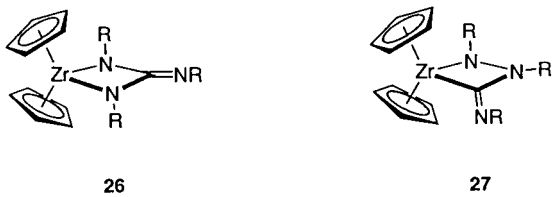

26 27

Figure 10. Two possible regioisomers, **26** and **27**.

Reactions of 1a−c with Carbodiimides. In the cycloaddition reactions of the zirconocene imido complexes Cp_2(THF)Zr=NR, R = *t*-Bu, 2,6-Me_2−C_6H_3, and 2,6-*i*-Pr_2−C_6H_3 (**1a**−**c**) with symmetrical carbodiimides, one of two possible regioisomers, **26** or **27** (Figure 10), could form. Methods such as NMR, MS, and elemental analysis would not allow us to differentiate between **26** and **27.** Therefore, a single-crystal X-ray crystallographic study was carried out on diazametallacycle **7a** (Figure 3). This revealed that a zirconium−nitrogen bond is formed in preference to a zirconium−carbon bond, resulting in regioisomer **26**.

Zirconium imido complex **1a** does not react with *t*-BuN=C=N-*t*-Bu, but it does react with Me_3SiN=C=$NSiMe_3$ to afford metallacycle **7d** (Table 4). These findings are attributed to steric effects since the nitrogen−carbon bond length in the N-*t*-Bu group is 1.429(5) Å and the nitrogen−silicon bond length in the N-$SiMe_3$ group is 1.675(3) Å from the crystallographic data obtained from **7d**.[37]

In analogy to the behavior of **1a**, treatment of the diisopropylphenyl complex **1b** with *t*-BuN=C=N-*t*-Bu gave no reaction at 25 °C or heating to 120 °C. This result was not surprising since **1b** is more sterically congested than **1a**. Treatment of **1b** with Me_3SiN=C=$NSiMe_3$ resulted in no reaction as well. However, **1b** reacts instantaneously at 25 °C with *i*-PrN=C=N-*i*-Pr and CycN=C=NCyc to afford metallacycles **9a** and **9b** (Table 4).

Scheme 7

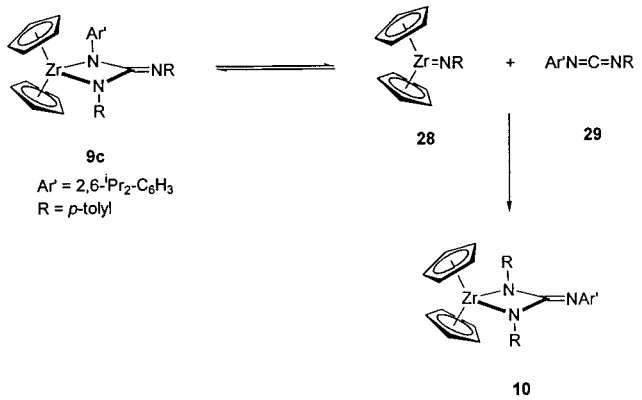

9c
Ar' = 2,6-^{i}Pr$_2$-C$_6$H$_3$
R = *p*-tolyl

28 29 10

Treatment of **1b** with *p*-tolylN=C=N-*p*-tolyl at 45 °C in C_6H_6 resulted in a new product after heating 4 days that is tentatively assigned as **9c** (Scheme 7) on the basis of spectroscopic data. Heating the reaction mixture at 75 °C for 15 h resulted in the further conversion of

(34) Cummins, C. C.; Baxter, S. M.; Wolczanski, P. T. *J. Am. Chem. Soc.* **1988**, *110*, 8731.
(35) Cummins, C. C.; Schaller, C. P.; Duyne, G. D. V.; Wolczanski, P. T.; Chan, A. W. E.; Hoffmann, R. *J. Am. Chem. Soc.* **1991**, *113*, 2985.
(36) Polse, J. L.; Andersen, R. A.; Bergman, R. G. *J. Am. Chem. Soc.* **1998**, *120*, 13405.

9c to one product, which has been isolated and characterized as the more thermodynamically stable zirconacycle **10**. This reaction could possibly occur by cycloreversion of **9c** to generate the unsymmetrical carbodiimide **29**. The newly formed zirconocene imido fragment $Cp_2Zr{=}N$-*p*-Tol **28** could then cycloadd to **29**, resulting in the formation of metallacycle **10**. Another possibility that cannot be ruled out at this point is an intramolecular rearrangement of zirconacycle **9c** to generate **10**.

We believe the driving force for the formation of **10** from **9c** is the relief of steric strain generated between the 2,6- *i*-Pr_2-C_6H_4 α to the zirconium metal center and the cyclopentadienyl ligands bound to zirconium. Breen and Stephan have reported the analogous reaction between $Cp_2Zr(PC_6H_2$-2,4,6- *t*-$Bu_3)(PMe_3)$ (**30**) and 1,3-dicyclohexylcarbodiimide to give metallacycle **32** (Scheme 8).[38] The intermediate metallacycle **31** was observed upon monitoring the reaction by ^{31}P NMR spectroscopy.

Scheme 8

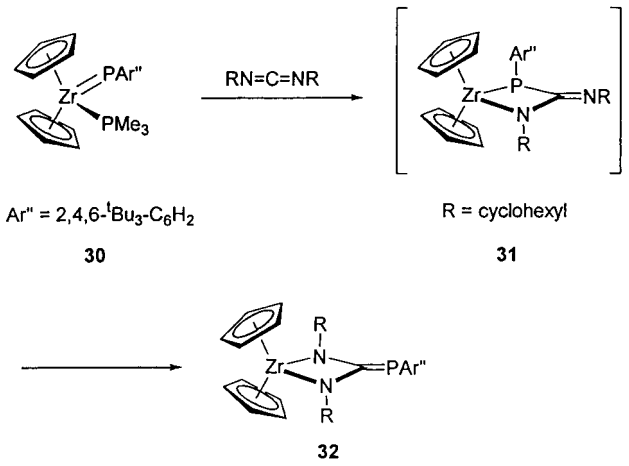

Carbodiimide Metathesis. The zirconocene imido complexes with parent cyclopentadienyl ligands that have been prepared are limited to those with more bulky substituents on the nitrogen. In the N-aryl cases, attempts to prepare imido complexes with hydrogen atoms on the phenyl ring lead only to dimerized products.[29] However, when these unhindered N-arylimido complexes are generated in situ, they can be trapped with unsaturated organic molecules such as diphenylacetylene, and the resulting azametallacyclobutene complexes can be isolated in high yields.[33] These zirconacycles can be used as a precursors to the $Cp_2Zr{=}$NAr fragment, for example, in the catalytic metathesis reaction between different N-aryl imines.[13,14]

As in the aryl zirconocene imido cases, there are also limitations in the preparation of alkyl imido complexes. All isolated compounds with the general formula Cp_2-(THF)Zr=NR (R = alkyl group) have no β hydrogens. This is because the (alkyl)(imido)zirconocene precursors undergo preferential β (rather than α) CH_4 elimination to give azametallacyclopropanes instead of imido complexes.[39] Because of their tendency to undergo retro [2 + 2] fragmentation, we saw that complexes such as **7a** might be potential alternate precursors to transient Cp_2-Zr=NR fragments having R groups with hydrogens on the N-bound carbon atom, as long as the appropriate carbodiimides are available. Trapping these species would allow us to generate new zirconacycles that would be difficult to prepare by other means. When complex **7a** was treated with 2 equiv of *i*-PrN=C=N-*i*-Pr, the symmetrical metallacycle **14** was obtained with the concurrent formation of *i*-PrN=C=N-*t*-Bu (eq 9). The proposed pathway for this transformation is outlined in Scheme 9. Metallacycle **7a** can undergo cycloreversion

Scheme 9

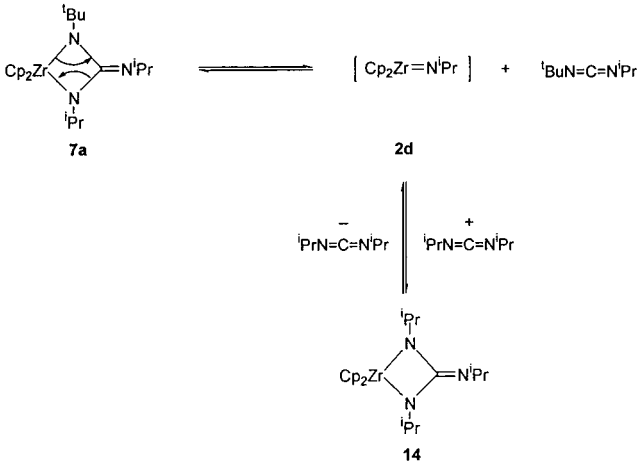

in one of two directions: in a reverse fashion or in a productive fashion to afford the new imido fragment $Cp_2Zr{=}N$-*i*-Pr (**2d**) and the extruded heterocumulene *i*-PrN=C=N-*t*-Bu. The transient imido species **2d** can react in a formal [2 + 2] cycloaddition reaction with *i*-PrN=C=N-*i*-Pr to give **14**. We favor a dissociative mechanism for this process since kinetic studies with other diazametallacycles such as **7d** have shown that the zirconacycle complex undergoes exchange reactions with other carbodiimides via a dissociative pathway.[37] Attempts to study the kinetics of this system under pseudo-first-order conditions proved to be unsuccessful due to the appearance of another unidentified product that is formed when the reaction is carried out in the presence of a large excess of *i*-PrN=C=N^{t}Pr.

Complex **14** exhibits fluxional behavior, as shown in the ^1H NMR spectra in Figure 8. This fluxionality is best explained as due to syn/anti isomerism. In Figure 8 the methyl signals of the three N-bound *i*-Pr substituents are labeled A, B, and C. There is a barrier to syn/anti isomerization of the exocyclic *i*-Pr group at site C. This can be seen from the stack plot (Figure 8), which shows two distinct *i*-Pr methyl signals at sites A and B at −8 °C. As the temperature is elevated, coalescence between sites A and B is reached at 46 °C. Increasing the temperature resulted in sharpening to one distinct *i*-Pr group for sites A and B.

We did not see any spectroscopic evidence of fluxionality with the other metallacycles generated. For example, there was only one *t*-Bu resonance observed in the ^1H and ^{13}C NMR spectra of diazametallacycle complex **7a**, indicating that the exocyclic *i*-Pr group is pointing away from the *t*-Bu group exclusively. This is

(37) Zuckerman, R. L.; Bergman, R. G. Unpublished results.
(38) Breen, T. L.; Stephan, D. W. *J. Am. Chem. Soc.* **1995**, *117*, 11914.
(39) Barr, K. J.; Watson, B. T.; Buchwald, S. L. *Tetrahedron Lett.* **1991**, *32*, 5465.

Scheme 10

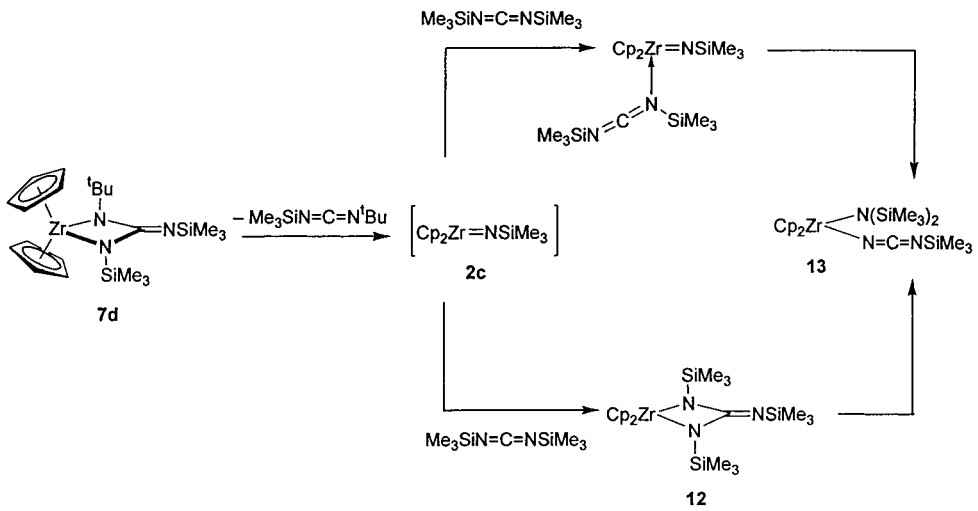

consistent with the results of the X-ray study of **7a** (Figure 3).

When diazametallacycle **7d** was treated with an excess of the symmetrical carbodiimide $Me_3SiN{=}C{=}NSiMe_3$, complex **13** was obtained (Scheme 3). Two mechanisms that seem reasonable for the formation of this organometallic compound are shown in Scheme 10. Both pathways involve initial cycloreversion to generate the zirconocene imido complex **2c** and the carbodiimide $Me_3SiN{=}C{=}N$-*t*-Bu. The reactive complex can undergo overall [2 + 2] cycloaddition to generate zirconacycle **12**. 1,3-Trimethysilyl migration with ring cleavage would then generate the observed product. The second pathway involves precoordination of the reactant carbodiimide to the zirconocene imido complex followed by 1,3-trimethysilyl migration. Currently we do not have the experimental information necessary to distinguish between these two pathways.

Conclusions

We have been able to generate organic carbodiimides from isothiocyanates through a zirconium-mediated heteroatom group transfer reaction with $Cp_2(THF)$-$Zr{=}N$-*t*-Bu. This transformation was found to be reasonably general, proceeding in good yield with several isothiocyanate substrates. The organometallic product obtained in all cases examined was $(Cp_2Zr(\mu S))_2$.

The NR group transfer reaction was further extended to carbodiimides ($RN{=}C{=}NR$). There are two processes necessary for heteroatom group transfer to be realized: addition of the zirconium imide fragment across the N=C double bond of the carbodiimide to generate a four-membered zirconacycle, and cycloreversion of this metallacycle to afford the metathesized heterocumulene and new Zr=NR moiety. Due to the stability of many of the zirconium-containing diazametallacycle products prepared and isolated, we were able to independently study the structural factors that are important in the overall [2 + 2] cycloaddition reaction. Steric factors in the cycloaddition reactions investigated were found to be significant in both the imido fragment and the heterocumulene reactant partner. Several of the metallacycle complexes prepared in the study were found to undergo further reaction with additional carbodiimide substrates to give metathesized products.

Experimental Section

General Comments. Unless otherwise noted, all manipulations were carried out under an inert atmosphere in a Vacuum Atmospheres 553-2 drybox with attached M6-40-^{1}H Dritrain or with use of standard Schlenk or vacuum line techniques. Degassed solutions were frozen to −196 °C, evacuated under high vacuum, and thawed.

Sealed NMR tubes (Wilmad 505-PP and 504-PP) were prepared by attaching Cajon adapters directly to Kontes vacuum stopcocks and flame sealing. J. Young tubes refer to resealable NMR tubes fitted with Teflon stopcocks. Glassware was dried in an oven at 150 °C before use. Pentane, hexanes, diethyl ether, toluene, benzene, and THF were distilled from Na/benzophenone. The solvents CH_2Cl_2 and $CHCl_3$ were distilled from CaH_2. The dueterated solvents C_6D_6, THF-d_8, and toluene-d_8 were purified by the same method as their protiated analogues and vacuum transferred prior to use. The reagents CS_2, 2,6-dimethylaniline, 2,6-diisopropylaniline, and 2,4,6-tri-*tert*-butylaniline were purchased from Aldrich, distilled from CaH_2, and stored over 4 Å sieves in the glovebox. Sieves (4 Å) were activated by heating under vacuum at 200 °C for 24 h. Methyl isothiocyanate, phenyl isothiocyanate, *tert*-butyl isothiocyanate, 1,3-dicyclohexylcarbodiimide, 1,3-diisopropylcarbodiimide, 1,3-di-*p*-tolylcarbodiimide, and 1,3-di-*tert*-butylcarbodiimide were purchased from Aldrich and were used without further purification. Imidozirconocene complexes **1a** and **1c** were synthesized according to literature procedures.[29]

All ^{1}H and $^{13}C\{^1H\}$ NMR spectra were recorded on commercial Bruker AMX 300 and 400 and DRX 500 spectrometers. Infrared spectra were recorded using a Mattson Instruments Galaxy 3000 Fourier transform spectrometer. Samples were prepared as Nujol mulls between NaCl plates. Mass spectrometric analyses were obtained at the University of California−Berkeley Mass Spectrometry Facility. Elemental analyses were performed at the University of California−Berkeley Microanalytical Facility on a Perkin-Elmer 2400 Series II CHNO/S analyzer.

$Cp_2(THF)Zr{=}N(2,6$-*i*-$Pr_2C_6H_3)$ (1b). Methyl amide **5a** (158 mg, 0.38 mmol) in THF (20 mL) was loaded into a 50 mL flask in the glovebox. The mixture was degassed with one freeze−pump−thaw cycle and heated at 95 °C for 2.5 days. The solvent was removed under reduced pressure, and the resulting brownish-red solid was diluted in toluene (2 mL). The solution was filtered through Celite, layered with hexanes (10 mL), and stored at −30 °C. Orange crystals were collected after 2 days (144 mg, 80% yield). ^{1}H NMR (THF-d_8): δ 6.71 (d, 2H, J = 3 Hz, aryl), 6.25 (t, 1H, J = 3 Hz, aryl), 6.14 (s, 10H, C_5H_5), 3.50 (m, 2H, $CH(CH_3)_2$), 1.14 (12H, J = 6 Hz, $CH(CH_3)_2$). $^{13}C\{^1H\}$ NMR (THF-d_8): δ 24.9 ($CH(CH_3)_2$), δ 27.4 ($CH(CH_3)_2$), δ 110.6

(C_5H_5), 115.5 (aryl), 122.2 (aryl), 136.7(aryl quat), 156.8 (N-aryl). IR (Nujol/NaCl): 3004, 2995, 2985, 2958, 2949, 2875, 2866, 2844, 2839, 1581, 1468, 1452, 1446, 1412,1379, 1334, 1273, 1255, 1138, 1099, 1006, 931, 858, 796, 781, 750, 719 cm^{-1}. Anal. Calcd for $C_{26}H_{35}ZrNO$: C, 66.62; H, 7.53; N, 2.99. Found: C, 66.44; H, 7.57; N, 2.94.

$Cp_2Zr(NH(2,6\text{-}(CH(CH_3)_2)_2C_6H_3))(CH_3)$ (5a). A solution of 2,6-diisopropylaniline (1.5 mmol, 261 mg) in diethyl ether (26 mL) was stirred at 25 °C in a 100 mL round-bottom flask, and *n*-butyllithium (2.2 M in hexanes, 0.68 mL) was added dropwise. The resulting yellow solution was stirred for 15 min, and $Cp_2Zr(CH_3)Cl$ (1.5 mmol, 400 mg) dissolved in diethyl ether (13 mL) was added. A white precipitate formed. The mixture was stirred at ca. 25 °C overnight. The mixture was filtered through Celite, and the solvent was removed under reduced pressure. The tan solid was triturated with diethyl ether to afford 400 mg (65% yield) of product that was pure by ^1H NMR analysis. A portion was doubly recrystallized from diethyl ether at −30 °C to obtain white crystals for elemental analysis. ^1H NMR (C_6D_6): δ 0.22 (s, 3H, CH_3), δ 1.2 (d, J = 6 Hz, CH-(CH_3)$_2$), δ 3.4 (m, 2H, CH), δ 5.8 (s, 10H, C_5H_5), δ 6.2 (s, 1H, NH), δ 7.1 (d, 2H, J = 3 Hz, aryl), δ 7.1 (m, 1H, aryl). $^{13}C\{^1H\}$ NMR (C_6D_6): δ 100.7, 111.2, 116.4, 122.3, 138.73, 155.9 (aryl), 110.0 (C_5H_5), 26.9 (*C*H), 25.4 (*C*H_3), δ 25.0 (Zr−*C*H_3). IR (Nujol/NaCl): 3311 w (ν_{NH}), 3087 w, 2723 w, 1726 w, 1710 w, 1691 w, 1627 w, 1583 w, 1319 m, 1241 m, 1226 w, 1195 m, 1014 m, 850 s, 798 m, 752 m, 684 w cm^{-1}. Anal. Calcd for $C_{23}H_{31}ZrN$: C, 66.93; H, 7.57; N, 3.39. Found: C, 66.54; H, 7.47; N, 3.23.

$Cp_2Zr(NH(2,4,6\text{-}(C(CH_3)_3)_3C_6H_2)(CH_3)$ (5b). $Cp_2Zr(CH_3)$-Cl (138 mg, 0.509 mmol) was dissolved in THF (2 mL). Lithium 2,4,6-*tert*-butylanilide (350 mg, 0.509 mmol) in THF (2 mL) was added dropwise. The mixture turned from clear to light yellow after the anilide addition was completed. After stirring at 25 °C overnight in an inert atmosphere, the solvent was removed under reduced pressure. Benzene (5 mL) was added to the resulting solid and filtered through Celite. The filtrate was concentrated under reduced pressure to leave a green solid (182 mg, 72% yield). Diethyl ether (2.5 mL) was added to the solid and stored at −30 °C for 1 day. Light green crystals were obtained in 61% isolated yield (154 mg) but showed slight impurities by ^1H NMR spectroscopy. The same crystallization procedure was repeated two more times to afford a sample for elemental analysis (120 mg, 47% yield). ^1H NMR (C_6D_6): δ 7.42 (s, 1H, aryl), 7.35 (s, 1H, aryl), 6.61 (1H, s, NH), 5.61 (s, 10H, C_5H_5), 1.57 (s, 9H, *t*-Bu), 1.39 (s, 9H, *t*-Bu), 1.37 (s, 9H, *t*-Bu), 0.22 (s, 3H, Zr−CH_3). $^{13}C\{^1H\}$ NMR (C_6D_6): δ 154.3, 144.5, 143.0, 141.7, 123.2, 120.6 (aryl), 110.2 (C_5H_5), 37.5, 36.5, 34.5 (*t*-Bu quat), 33.5, 31.8, 31.7 (*t*-Bu *C*H_3), 23.9 (Zr *C*H_3). IR (Nujol/NaCl): 3350 w, 3812 s, 2991 s, 2983 m, 2971 s, 2956 s, 2923 s, 2986 s, 2894 w, 2873 w, 2844 w, 2836 w, 1448 s, 1376 w, 1211 m, 808 m cm^{-1}. Anal. Calcd for $C_{29}H_{43}NZr$: C, 70.10; H, 8.72; N, 2.82. Found: C, 69.86; H, 8.83; N, 2.85.

Cyclometalated Product 6. $Cp_2Zr(NH(2,4,6\text{-}(C(CH_3)_3)_3$-$C_6H_2)(CH_3)$ (**5b**) (310 mg, 0.624 mmol) was dissolved in THF (10 mL) in a 25 mL reaction flask, and the solution was heated to 135 °C for 5 days. The solvent was evaporated under reduced pressure to leave a viscous orange oil, which was dissolved in Et_2O (2 mL) and stored at −35 °C. After 1 day, **6** was obtained as orange blocks (275 mg, 92% yield). ^1H NMR (C_6D_6): δ 7.55 (s, 1H, aryl), 7.34 (s, 1H, aryl), 5.64 (s, 10H, C_5H_5), 1.65 (s, 6H, CH_3), 1.42 (s, 9H, C(CH_3)$_3$), 1.37 (s, 9H, C(CH_3)$_3$). Anal. Calcd for $C_{28}H_{39}NZr$: C, 70.11; H, 8.20; N, 2.92. Found: C, 70.21; H, 8.23; N, 2.99.

Reaction of Cp_2(THF)Zr=N-*t*-Bu (1a) with CS_2. A J. Young NMR tube was charged with Cp_2(THF)Zr=N-*t*-Bu (**1a**) (6.7 mg, 0.018 mmol), ferrocene (4.0 mg, 0.022 mmol), and 0.5 mL of C_6D_6. A single-pulse ^1H NMR spectrum was acquired in which the resonance of the cyclopentadienyl ligands and *tert*-butyl group were integrated against the cyclopentadienyl ligands of the ferrocene. CS_2 (1.9 mg, 1.5 μL, 0.025 mmol) was added to the NMR tube at 25 °C in the glovebox, and the solution turned from light orange to lime green within seconds after the addition. After 20 min, another ^1H NMR spectrum was obtained as described above; a 95% yield of sulfido dimer **3** was measured. ^1H NMR spectrometry indicated that 1,3-di-*tert*-butylcarbodiimide (δ 1.16 in C_6D_6) was formed in 10% yield and *tert*-butyl isothiocyanate (δ -0.79 in C_6D_6, was formed in 73% yield by integration against the internal standard. The volatile materials were collected using standard Schlenk line transfer methods. The ^1H NMR spectrum and GC/MS of the 1,3-di-*tert*-butylcarbodiimide and *tert*-butyl isothiocyanate were identical to those of authentic samples purchased from Aldrich. The resulting solid (91% yield) was analyzed by ^1H NMR spectrometry and mass spectrometry. MS(EI) *m/e* 506 for $(Cp_2ZrS)_2$ (**3**). ^1H NMR ($CDCl_3$): δ 6.26 (s, 20H, C_5H_5). Lit.[28] ^1H NMR ($CDCl_3$): δ 6.26 (s, 20H, C_5H_5) for $(Cp_2ZrS)_2$ (**3**).

Reaction of Cp_2(THF)Zr=N-*t*-Bu (1a) with *tert*-Butyl Isothiocyanate. A J.Young NMR tube was charged with Cp_2-(THF)Zr=N-*t*-Bu (**1a**) (10 mg, 0.027 mmol) and ferrocene (3 mg, 0.016 mmol) in 0.5 mL of C_6D_6. A single-pulse ^1H NMR spectrum was acquired in which the resonance of the cyclopentadienyl ligands and *tert*-butyl group were integrated against the cyclopentadienyl ligands of the ferrocene. In the glovebox, *tert*-butyl isothiocyanate (4.3 mg, 4.4 μL, 0.037 mmol) was added to the J. Young tube. The solution turned light green within 5 min after the addition. Another single-pulse ^1H NMR spectrum was acquired. Using this technique, it was determined that $(Cp_2ZrS)_2$ (**3**) was formed in 88% yield. ^1H NMR spectrometry indicated that 1,3-di-*tert*-butylcarbodiimide (δ 1.16 in C_6D_6) was formed in 93% yield by integration against the internal standard. The volatile materials were collected in another NMR tube using standard Schlenk line transfer methods. The ^1H NMR spectrum and GC/MS of the 1,3-di-*tert*-butylcarbodiimide were identical to those of an authentic sample purchased from Aldrich.

Reaction of Cp_2(THF)Zr=N-*t*-Bu (1a) with Phenyl Isothiocyanate. The same general procedure was used as the one described for the reaction of **1a** and *tert*-butyl isothiocyanate. A J. Young NMR tube was charged with Cp_2(THF)-Zr=N-*t*-Bu (**1a**) (11.0 mg, 0.03 mmol) and ferrocene (6.2 mg, 0.033 mmol) in 0.5 mL of C_6D_6. Phenyl isothiocyanate (5.6 mg, 5 μL, 0.04 mmol) was added to the NMR tube. The reaction mixture turned purple immediately, but after 15 min, the mixture began to turn from purple to green. After 24 h, the mixture was brownish-green in color. It was determined that $(Cp_2ZrS)_2$ (**3**) was formed in 96% yield by integration against the internal standard ferrocene. The volatile materials were collected in another NMR tube using Schlenk line transfer methods and analyzed by GC/MS. The identification of PhN=C=N-*t*-Bu was confirmed by mass spectrometry.

Reaction of Cp_2(THF)Zr=N-*t*-Bu (1a) with Methyl Isothiocyanate. Cp_2(THF)Zr=N-*t*-Bu (**1a**) (4.5 mg, 0.012 mmol) and ferrocene (2.9 mg, 0.015 mmol) in 0.5 mL of C_6D_6 were added to a J. Young NMR tube. The same general procedure was used as the one described for the reaction of **1a** and *tert*-butyl isothiocyanate. Methyl isothiocyanate (1.24 mg, 0.02 mmol) was added to the NMR tube in the glovebox. The solution turned a dark yellow after methyl isothiocyanate was added. Analysis of the reaction mixture by ^1H NMR spectrometry showed the formation of two products. Sulfido dimer **3** formed in 77% yield, and an unknown compound was observed in 14% yield calculated from integration with the internal standard. The mixture was heated at 45 °C for 2 h followed by heating at 96 °C for 22 h to give sulfido dimer **3** in 91% yield. The volatile materials were collected and analyzed by GC/MS. 1-Methyl-3-*tert*-butylcarbodiimide was identified by mass spectrometry as the organic product produced in the reaction.

$Cp_2Zr(N(t\text{-}Bu)C{=}N(i\text{-}Pr)N(i\text{-}Pr))$ (7a). A flask was charged with imido complex **1a** (110 mg, 0.300 mmol) and C_6H_6 (20 mL). While stirring the mixture, 1,3-diisopropylcarbodiimide (65.2 μL, 0.400 mmol) was added dropwise. The solution turned

purple immediately. The mixture was stirred at 25 °C under N_2 for 1 h followed by removal of the solvent under reduced pressure to afford a purple solid. The material was dissolved in hexanes (4 mL), and the solvent slowly evaporated over 2 days. Purple crystals were obtained (121 mg, 97% yield). ^{1}H NMR (C_6D_6): δ 6.04 (s, 10H, C_5H_5), 4.1 (m, 1H, CH(CH$_3$)$_2$), 1.5 (s, 9H, C(CH_3)$_3$), 1.4 (d, J = 6 Hz, 6H, CH(CH_3)$_2$), 0.93 (d, J = 6 Hz, 6H, CH(CH_3)$_2$). ^{13}C{^{1}H} NMR (C_6D_6): δ 25.6 (*t*-Bu CH_3's), 27.6, 30.9 (*i*-Pr CH_3's), 44.7, 48.7 (*i*-Pr CH's), 55.6 (*t*-Bu quat), 114.12 (C_5H_5), 138.7 (C=N quat). IR (Nujol/NaCl): 2975 s, 2935 s, 2925 s, 2898 w, 2871 w, 2834 w, 1564 s, 1552 s, 1355 m, 1223 s, 792 s, 524 w, 516 m, 489 m, 458 m cm^{-1}. Anal. Calcd for $C_{21}H_{31}N_3Zr$: C, 60.24; H, 7.94; N, 10.04. Found: C, 60.45; H, 8.00; N, 9.92.

Cp$_2$Zr(N(*t*-Bu)C=N(cyclohexyl)N(cyclohexyl)) (7b). A glass reaction vessel equipped with a Teflon stopcock was charged with Cp$_2$(THF)Zr=N-*t*-Bu (**1a**) (109 mg, 0.300 mmol) and C_6H_6 (30 mL). The mixture was stirred at 25 °C, and 1,3-dicyclohexylcarbodiimide (82.5 mg, 0.4 mmol) was added. The mixture turned purple immediately. After stirring 1 h, the solvent was removed under reduced pressure to afford a purple solid. The solid was crystallized from toluene layered with hexanes and stored at −30 °C for 2 days to afford purple crystals (58 mg, 81% yield). ^{1}H NMR (C_6D_6): δ 6.07 (s, 10H, C_5H_5), δ 3.75 (m, 1H, CH), δ 3.60 (m, 1H, CH), δ 1.50 (s, 9H, C(CH_3)$_3$), δ 0.68 - 2.38 (m, 20H, cyclohexyl CH_2's). ^{13}C{^{1}H} NMR (C_6D_6): δ 25.8, 26.0, 26.42, 26.9, 30.7, 36.2, 37.9, 53.2, 55.3, 58.0, 114.0, 129.0. IR ($\nu_{C=N}$): 1348 m, 1254 m, 1217 vs, 1186 m, 1016 m, 987 w, 792 s cm^{-1}. Anal. Calcd for $C_{27}H_{41}N_3Zr$: C, 65.01; H, 8.28; N, 8.42. Found: C, 64.78; H, 8.35; N, 8.10.

Cp$_2$Zr(N(*t*-Bu)C=N(Tol)N(Tol)) (7c). A glass reaction vessel equipped with a Teflon stopcock was charged with Cp$_2$(THF)Zr=N-*t*-Bu (**1a**) (257 mg, 0.70 mmol) and 10 mL of C_6H_6. The solution was stirred, and 1,3-di-*p*-tolylcarbodiimide (156 mg, 0.70 mmol) was added dropwise. The solution turned from yellow to royal blue immediately. After stirring at 25 °C for 20 min, the solvent was removed under reduced pressure to afford a blue solid. The solid was crystallized from benzene layered with hexanes at 25 °C for 2 days to afford royal blue needle crystals (259 mg, 72% yield). ^{1}H NMR (C_6D_6): δ 7.11 (d, J = 3 Hz, 2H, aryl), δ 6.98 (d, J = 3 Hz, 2H, aryl), δ 6.83 (d, J = 3 Hz, 2H, aryl), δ 6.46 (d, J = 3 Hz, 2H, aryl), δ 5.95 (s, 10H, C_5H_5), δ 2.06 (s, 3H, CH_3), δ 2.01 (s, 3H, CH_3), δ 1.48 (s, 9H, C(CH_3)$_3$). ^{13}C{^{1}H} NMR (C_6D_6): δ 148.3, 148.1 (aryl), 142.5 (quat), 128.7, 128.7, 127.5, 127.1, 122.5, 120.3 (aryl), 54.8 (*t*-Bu quat), 29.9 (*t*-Bu CH$_3$'s), 20.7, 20.5 (aryl CH$_3$'s). IR (Nujol/NaCl): 2954, 2942, 2929, 2919, 2988, 2892, 2871, 2860, 2848, 1521, 1506, 1460, 1377, 1315, 1245, 1223, 968, 806 cm^{-1}. Anal. Calcd for $C_{29}H_{33}N_3Zr$: C, 67.66; H, 6.46; N, 8.16. Found: C, 67.99; H, 6.64; N, 7.86.

Cp$_2$Zr(N(*t*-Bu)C=N(SiMe$_3$)N(SiMe$_3$)) (7d). A glass reaction vessel equipped with a Teflon stopcock was charged with Cp$_2$(THF)Zr=N-*t*-Bu (**1a**) (309 mg, 0.84 mmol) and 10 mL of C_6H_6. The solution was stirred, and 1,3-bis(trimethylsilyl)-carbodiimide (174 mg, 211 μL, 0.93 mmol) was added dropwise, upon which the solution turned from orange to red immediately. After stirring at 25 °C for 2 h, the solvent was removed under reduced pressure to afford a red solid in 99% yield (398 mg). The solid was crystallized from hexanes at −30 °C to afford deep red crystals (181 mg, 45% yield). ^{1}H NMR (C_6D_6): δ 5.98 (s, 10H, C_5H_5), 1.16 (s, 9H, C(CH_3)$_3$), 0.56 (s, 9H, Si(CH_3)$_3$), 0.22 (s, 9H, Si(CH_3)$_3$). ^{13}C{^{1}H} NMR (C_6D_6): δ114.8 (C_5H_5), 82.4 (quat), 53.3 (*t*-Bu quat), 30.1 (*t*-Bu CH_3's), 5.0, 2.4 (Si CH_3's). IR (Nujol/NaCl): 2972 m, 2958 m, 2941 m, 2900 vs, 2891 m, 2883 m, 2870 m, 2854 m, 2843 m, 1583 m, 1462 m, 1452 w, 1377 w, 1236 m, 866 m, 833 m, 816 m, 796 w, 758 w cm^{-1}. Anal. Calcd for $C_{21}H_{37}N_3Si_2Zr$: C, 52.66; H, 7.79; N, 8.77. Found: C, 52.40; H, 7.97; N, 8.62.

Cp$_2$Zr(N(2,6-*i*-Pr$_2$C$_6$H$_3$)C=N(*i*-Pr)N(*i*-Pr)) (9a). A glass reaction vessel equipped with a Teflon stopcock was charged with zirconocene imido complex **1b** (194 mg, 0.440 mmol) and 7 mL of C_6H_6. The solution was stirred, and 1,3-diisopropylcarbodiimide (52.3 mg, 65.0 μL, 0.44 mmol) was added dropwise. The solution turned from orange to purple immediately. After stirring at 25 °C for 1 h, the solvent was removed under reduced pressure to afford a purple solid. The solid was crystallized from hexanes (189 mg, 82% yield). ^{1}H NMR (C_6D_6): δ 7.14 (d, 2H, J = 3 Hz, aryl), 7.09 (t, 1H, J = 3 Hz, aryl), 6.02 (s, 10H, C_5H_5), 4.01 (m, 2H, CH(CH$_3$)$_2$), 3.41 (m, 2H, CH(CH$_3$)$_2$), 1.43 (d, J = 6 Hz, 6H, CH(CH_3)$_2$), 1.18 (d, J = 6 Hz, 6H, CH(CH_3)$_2$), 1.10 (d, J = 6 Hz, 6H, CH(CH_3)$_2$). ^{13}C-{^{1}H} NMR (C_6D_6): δ 141.4, 127.5, 123.9, 122.8, 109.6, 109.1 (aryl), 114.7 (C_5H_5), 54.0, 36.3, 35.1, 34.7, 27.3, 26.9, 26.6, 25.6, 25.6, 23.6. IR (Nujol/NaCl): 2960 vs, 2918 s, 2927 vs, 2860 m, 2243 vw, 1500 m, 1462 m, 1402 m, 1203 s, 1037 m, 866 vw cm^{-1}. Anal. Calcd for $C_{29}H_{41}N_3Zr$: C, 66.61; H, 7.90; N, 8.04. Found: C, 66.37; H, 8.03; N, 7.87.

Cp$_2$Zr(N(2,6-*i*-Pr$_2$C$_6$H$_3$)C=N(cyclohexyl)N(cyclohexyl)) (9b). A glass reaction vessel equipped with a Teflon stopcock was charged with zirconocene imido complex **1b** (194 mg, 0.44 mmol) and 7 mL of C_6H_6. The solution was stirred, and 1,3-dicyclohexylcarbodiimide (52.3 mg, 65.0 μL, 0.44 mmol) was added dropwise, upon which the solution turned from orange to purple. After stirring at 25 °C for 1 h under nitrogen, the solvent was removed under reduced pressure to afford a purple solid. The solid was crystallized from hexanes solution to give **9b** (190 mg, 72% yield). ^{1}H NMR (C_6D_6): δ 7.14 (d, 2H, aryl), 7.95 (t, 1H, aryl), 6.07 (s, 10H, C_5H_5), 3.78 (m, 1H, cyclohexyl methine), 3.59 (m, 2H, cyclohexyl methine), 2.95 (m, 1H, cyclohexyl methine). ^{13}C{^{1}H} NMR (C_6D_6): δ 141.4, 123.8, 122.8, 105.6, 114.7, 105.1, 54.0, 36.3, 35.1, 34.7, 27.3, 26.9, 26.6, 25.6, 25.6, 23.6. IR (Nujol/NaCl): 3002 s, 2983 vs, 2973 s, 2964 m, 2946 s, 2935 s, 2918 vw, 2858 vw, 2832 w, 1558 vw, 1544 vw, 1469 s, 1456 m, 1448 m, 1359 m, 1249 w, 796 s cm^{-1}. Anal. Calcd for $C_{35}H_{49}N_3Zr$: C, 69.71; H, 8.19; N, 6.97. Found: C, 69.53; H, 8.17; N, 6.85.

Cp$_2$Zr(N(2,6-*i*-Pr$_2$C$_6$H$_3$)C=N(Tol)N(Tol)) (9c). A glass reaction vessel equipped with a Teflon stopcock was charged with zirconocene imido complex **1b** (110 mg, 0.23 mmol) and 7 mL of C_6H_6. The solution was stirred as 1,3-di-*p*-tolylcarbodiimide (52.3 mg, 0.23 mmol) was added dropwise. The solution turned brown in color immediately. After heating for 3 days at 45 °C, the solution had turned from brown to purple in color. The resulting product is tentatively identified as diazametallacycle **9c** based on the ^{1}H NMR spectrum and was carried on without isolation. ^{1}H NMR (C_6D_6): δ 7.1−6.8 (m, 11H, aryl), 6.0 (s, 10H, C_5H_5), 3.45 (m, 2H, CH(CH$_3$)$_2$), 2.15 (s, 3H, CH_3), 2.08 (s, 3H, CH_3), 1.46 (d, J = 6 Hz, 6H, CH(CH_3)$_2$), 1.20 (d, J = 6 Hz, 6H, CH(CH$_3$)$_2$).

Cp$_2$Zr(N(*i*-Pr)C=N(2,6-*i*-Pr$_2$C$_6$H$_3$)N(*i*-Pr)) (10). A crude solution of **9c** from above was heated to 75 °C for 15 h. The solvent was removed at reduced pressure to afford a purple solid (143 mg, 96% yield). The solid was dissolved in hexanes (2 mL) and stored at −35 °C for 6 days to yield purple crystals (127 mg, 89% yield). ^{1}H NMR (C_6D_6): δ 6.9−7.1 (m, 11H, aryl), 5.96 (s, 10H, C_5H_5), 3.75 (m, 2H, CH(CH$_3$)$_2$), 2.15 (s, 6H, CH_3), 1.44 (d, J = 1.2 Hz, 12H, CH(CH_3)$_2$). ^{13}C{^{1}H} NMR (C_6D_6): δ 146.76, 144.95, 137.9, 129.83, 128.97, 128.29, 122.59, 120.99, 120.65, 115.72, 28.91, 23.63, 20.84. Anal. Calcd for $C_{37}H_{41}N_3Zr$: C, 71.8; H, 6.68; N, 6.79. Found: C, 72.02; H, 6.79; N, 6.61.

Cp$_2$Zr(N(2,6-Me$_2$C$_6$H$_3$)C=N(*i*-Pr)N(*i*-Pr)) (11a). A glass reaction vessel equipped with a Teflon stopcock was charged with Cp$_2$(THF)Zr=N(2,6-Me$_2$C$_6$H$_3$) (**1c**) (150 mg, 0.36 mmol) and 5 mL of C_6H_6. To this solution was added 1,3-diisopropylcarbodiimide (46 mg, 0.36 mmol) dropwise with stirring, and a color change from orange to purple was noted. Stirring was continued for 1 h at 25 °C. Removing the solvent at reduced pressure left a purple solid, which was dissolved in toluene (1 mL), layered with hexanes (4 mL), and stored at −35 °C for 1 day to give purple blocks (146 mg, 92% yield). ^{1}H NMR (C_6D_6): δ 7.18 (d, J = 3 Hz, 2H, aryl), 6.96 (t, J = 3 Hz, 1H,

aryl), 5.80 (s, 10H, C_5H_5), 4.01 (m, 1H, C*H*$(CH_3)_2$), 2.21 (s, 6H, aryl C*H*$_3$'s), 1.32 (d, J = 6 Hz, 6H, CH(C*H*$_3$)$_2$, 1.18 (d, J = 6 Hz, 6H, CH(C*H*$_3$)$_2$. $^{13}C\{^1H\}$ NMR (C_6D_6): δ 151.9, 129.3, 128.8, 121.9, 114.2, 47.5, 46.0, 26.2, 24.4, 21.1. Anal. Calcd for $C_{25}H_{30}N_3Zr$: C, 64.33; H, 7.13; N, 9.00. Found: C, 64.25; H, 7.16; N, 8.77.

Cp$_2$Zr(N(2,6-Me$_2$C$_6$H$_3$)C═N(cyclohexyl)N(cyclohexyl)) (11b). 1,3-Dicyclohexylcarbodiimide (48 mg, 0.23 mmol) was added to a solution of zirconocene imido complex **1c** (96 mg, 0.23 mmol) in C_6H_6 (5 mL). A color change from orange to purple was noted. After stirring at 25 °C for 1 h, the solvent was removed at reduced pressure to leave an indigo solid. This was dissolved in Et_2O (2 mL) and stored at −35 °C for 1 day to give purple crystals (112 mg, 88% yield). ^1H NMR (C_6D_6): δ 7.18 (d, J = 3 Hz, 2H, aryl), 6.96 (t, J = 3 Hz, 1H, aryl), 5.80 (s, 10H, C_5H_5), 2.21 (s, 6H, aryl C*H*$_3$'s), 3.09 (m, 2H, cyclohexyl methines), 2.21 (s, 6H, aryl C*H*$_3$'s), 1.85−1 (cyclohexyl C*H*$_2$). $^{13}C\{^1H\}$ NMR (C_6D_6): δ 152.04, 129.2, 129.1, 121.1, 114.9, 54.8, 36.7, 34.8, 27.1, 26.8, 25.9, 25.8, 21.1. Anal. Calcd for $C_{27}H_{41}N_3Zr$: C, 68.08; H, 7.56; N, 7.68. Found: C, 67.91; H, 7.47; N, 7.41.

Cp$_2$Zr(N(2,6-Me$_2$C$_6$H$_3$)C═N(Tol)N(Tol)) (11c). 1,3-Di-*p*-tolylcarbodiimide (67 mg, 0.30 mmol) was added to a stirring solution of zirconocene imido complex **1c** (124 mg, 0.30 mmol) in C_6H_6 (0.5 mL). The solution turned from orange in color to a dark indigo when 1,3-di-*p*-tolylcarbodiimide was added. The solution continued stirring at 25 °C for 1 h, and the solvent was removed at reduced pressure to afford a powder. The solid was dissolved in hexanes (2 mL) and stored at −35 °C, upon which indigo crystals formed in 89% yield (150 mg). ^1H NMR (C_6D_6): δ 7.56 (d, J = 3 Hz, 2H, aryl), 6.96 (t, J = 3 Hz, 1H, aryl), 5.92 (s, 10H, C_5H_5), 2.27 (s, 3H, C*H*$_3$), 2.17 (s, 6H, C*H*$_3$), 2.08 (s, 3H, C*H*$_3$). $^{13}C\{^1H\}$ NMR (C_6D_6): δ 148.7, 148.3, 147.1, 130.1, 129.2, 128.8, 128.5, 128.3, 122.2, 122.1, 121.0, 115.9, 21.2, 21.0, 20.9. Anal. Calcd for $C_{33}H_{33}N_3Zr$: C, 70.42; H, 5.91; N, 7.47. Found: C, 70.06; H, 5.94; N, 7.29.

Cp$_2$Zr(N(2,6-Me$_2$C$_6$H$_3$)C═N(SiMe$_3$)N(SiMe$_3$)) (11d). Cp$_2$(THF)Zr═N(2,6-Me$_2$C$_6$H$_3$) (**1c**) (151 mg, 0.37 mmol) and 1,3-bis(trimethylsilyl)carbodiimide (68 mg, 83 μL, 0.93 mmol) were dissolved in 5 mL of C_6H_6. A red color developed immediately. The mixture was stirred at 25 °C for 1 h. Removing the solvent at reduced pressure left a red solid. The crude solid was dissolved in Et_2O (2 mL) and stored at −35 °C for 3 days to give red blocky crystals (140 mg, 73% yield). ^1H NMR (C_6D_6): δ 7.18 (d, J = 3 Hz, 2H, aryl), 6.96 (t, J = 3 Hz, 1H, aryl), 5.80 (s, 10H, C_5H_5), 2.21 (s, 6H, aryl C*H*$_3$), 0.11 (s, 9H, TMS), 0.05 (s, 9H, Si(C*H*$_3$)$_3$). $^{13}C\{^1H\}$ NMR (C_6D_6): δ 148.5 (quat), 132.4, 129.3, 122.9 (aryl), 115.6 C_5H_5, 21.2 (aryl CH_3), 2.6 and 1.8 (Si(*C*H$_3$)$_3$). Anal. Calcd for $C_{25}H_{37}Si_2N_3Zr$: C, 56.98; H, 7.08; N, 7.97. Found: C, 56.73; H, 7.05; N, 7.59.

Cp$_2$Zr(N(2,6-Me$_2$C$_6$H$_3$)C═N(Tol)N(Tol)) (11e). Cp$_2$(THF)Zr═N(2,6-Me$_2$C$_6$H$_3$) (**1c**) (225 mg, 0.54 mmol) and 1,3-di-*tert*-butylcarbodiimide (84 mg, 0.54 mmol) were dissolved in 5 mL of C_6H_6. A purple color developed immediately. The mixture was stirred at 25 °C for 1 h. Removing the solvent at reduced pressure left a purple solid, which was dissolved in hexanes (3 mL) and stored at −35 °C for 1 day to give purple crystals (234 mg, 87% yield). ^1H NMR (C_6D_6): δ 7.08 (d, J = 3 Hz, 2H, aryl), 7.03 (t, J = 3 Hz, 1H, aryl), 5.98 (s, 10H, C_5H_5), 2.24 (s, 6H, aryl C*H*$_3$'s), 1.39 (s, 9H, (C*H*$_3$)$_3$), 1.27 (s, 9H, (C*H*$_3$)$_3$). $^{13}C\{^1H\}$ NMR (C_6D_6): δ 154.0, 138.4, 129.7, 129.6, 128.5, 120.9, 115.0, 54.7, 52.5, 32.0, 31.5, 29.6, 21.7. Anal. Calcd for $C_{27}H_{41}N_3Zr$: C, 65.01; H, 8.28; N, 8.42. Found: C, 64.78; H, 8.35; N, 8.10.

Cp$_2$Zr(N(SiMe$_3$)$_2$(N═C═NSiMe$_3$) (13). Cp$_2$(THF)Zr═N-*t*-Bu (**1a**) (118 mg, 0.32 mmol) and 1,3-bis(trimethylsilyl)-carbodiimide (603 mg, 734 μL, 3.23 mmol) were dissolved in 7 mL of C_6H_6. A red color due to the formation of **7d** developed immediately. The mixture was heated at 80 °C for 10 h followed by the removal of solvent at reduced pressure to leave a light yellow solid (147 mg, 92% yield). The solid was dissolved in a hexanes solution (2 mL) and stored at −35 °C for 2 days to afford yellow blocky crystals (136 mg, 85% yield). ^1H NMR (C_6D_6): δ 5.95 (s, 10H, C_5H_5), 0.39 (s, 9H, Si(C*H*$_3$)$_3$), 0.30 (s, 9H, Si(C*H*$_3$)$_3$), 0.20 (s, 9H, Si(C*H*$_3$)$_3$). $^{13}C\{^1H\}$ NMR: δ 113.7 (C_5H_5), 6.9 ((*C*H$_3$)$_3$), 6.4 ((*C*H$_3$)$_3$), 1.9 ((*C*H$_3$)$_3$), quat not found. Anal. Calcd for $C_{20}H_{37}N_3Si_3Zr$: C, 48.67; H, 7.56; N, 8.52. Found: C, 48.59; H, 7.61; N, 8.30.

Cp$_2$Zr(N(*i*-Pr)C═N(*i*-Pr)N(*i*-Pr)) (14). Cp$_2$(THF)Zr═N-*t*-Bu (**1a**) (110 mg, 0.30 mmol) and 1,3-diisopropylcarbodiimide (115 mg, 142 μL, 0.90 mmol) were dissolved in 5 mL of C_6H_6. A purple color developed immediately. The mixture was stirred at 25 °C overnight. The solvent was removed at reduced pressure to leave a purple solid, which was dissolved in hexanes (2 mL) and stored at −35 °C for 2 days to afford purple needles (98 mg, 81% yield). ^1H NMR (46 °C, C_6D_6): δ 6.05 (s, 10H, C_5H_5), 4.30 (m, 2H, C*H*$(CH_3)_2$), 4.17 (m, 1H, C*H*$(CH_3)_2$), 1.39 (d, J = 6 Hz, 6H, CH(C*H*$_3$)$_2$), 1.10 (d, J = 6 Hz, 12H, CH(C*H*$_3$)$_2$). $^{13}C\{^1H\}$ NMR (46 °C, C_6D_6): δ 137.22 (quat), 113.86 (C_5H_5), 47.3 (*C*H$(CH_3)_2$), 44.1 (*C*H$(CH_3)_2$), 27.3 (CH(*C*H$_3$)$_2$), 25.1 (CH(*C*H$_3$)$_2$). Anal. Calcd for $C_{20}H_{31}N_3Zr$: C, 59.36; H, 7.72. Found: C, 59.00; H, 7.52.

X-ray Structure Determination of 1b, 6, 7a, 9a, and 13. All crystals were mounted on quartz fibers using Paratone N hydrocarbon oil. For all compounds, measurements were made on a SMART CCD area detector with graphite monochromated Mo Kα radiation. Data were integrated by the program SAINT. The data were corrected for Lorentz and polarization effects and analyzed for agreement and possible absorption using XPREP.[40] An empirical absorption correction based on comparison of redundant and equivalent reflections was applied using SADABS[41] (**1b**, T_{max} = 0.88, T_{min} = 0.74; **6**, T_{max} = 0.93, T_{min} = 0.73; **7a**, T_{max} = 0.93, T_{min} = 0.82; **9a**, T_{max} = 0.90, T_{min} = 0.81; **13**, T_{max} = 0.87, T_{min} = 0.79). The structures were solved by direct methods and expanded using Fourier techniques. The non-hydrogen atoms were refined anisotropically. Plots of $\sum w(|F_o| - |F_c|)^2$ versus $|F_o|$, reflection order in data collection, $(\sin\theta)/\lambda$, and various classes of indices showed no unusual trends. All calculations were performed using the teXsan[42] crystallographic software package of Molecular Structure Corp.

Crystallographic data for compounds **1b**, **6**, **7a**, **9a**, and **13** and selected bond lengths and bond angles are given in Tables 1−3 and 5−9; full details are given in the Supporting Information.

Acknowledgment. The authors thank Drs. Frederick Hollander and Patricia Goodson for solving the crystal structures of **1b**, **6**, **7a**, **9a**, and **13**, the National Institutes of Health (Grant No. GM-25459) for financial support of this work, and Prof. Kristopher McNeill (University of Minnesota) for fruitful discussions.

Supporting Information Available: Crystallographic data for **1b**, **6**, **7a**, **9a**, and **13** are available. This material is available free of charge via the Internet at http://pubs.acs.org.

OM000614C

(40) *XPREP*, v. 5.03 (part of the SHELXTL Crystal Structure Determination Package); Siemens Industrial Automation, Inc., 1995.
(41) Sheldrick, G. *SADABS*: Siemens Area Detector Absorption correction program; Siemens Industrial Automation, Inc., 1996.
(42) *teXsan*: Crystal Structure Analysis Package; Molecular Structure Corp., 1985 and 1992.